

**Supplementary Information for:**

**Photo-mechanical azobenzene cocrystals and in situ X-ray  
diffraction study of their optically-induced crystal-to-crystal  
isomerisation**

Oleksandr S. Bushuyev, T. Christopher Corkery, Christopher J. Barrett and Tomislav Friščić

Department of Chemistry and FRQNT Centre for Self-Assembled Chemical Structures, McGill University, 801  
Sherbrooke St. W., H3A 0B8, Montreal, Canada

**Table of Contents**

<b>1. Experimental</b>	2
1.1 Materials	2
1.2 Cocrystals preparation	2
<b>2. Single crystal X-ray diffraction measurements and crystallographic summary</b>	4
<b>3. Photo-mechanical motion measurements</b>	6
<b>4. Summary of indexing the crystal of (<i>cis</i>-2)(<i>cis</i>-bpe) after irradiation</b>	7
<b>5. Powder X-ray diffraction data</b>	9
<b>6. Thermal analysis data</b>	10
<b>7. Vibrational analysis data</b>	19
<b>8. References</b>	28

## 1. Experimental

### 1.1 Materials:

4,4'-dibromooctafluoroazobenzene (**1**) and 4-iodo-2,3,5,6-tetrafluoroaniline(**2**) were synthesized and as outlined in our prior report which also reported their spectroscopic properties, including UV/Vis spectra and  $K$ ,  $t_{1/2}$  and molar extinction coefficient values in different solvents.<sup>1</sup> Precursors such as 4-bromo-2,3,5,6-tetrafluoroaniline, 2,3,5,6-tetrafluoroaniline and mercury oxide were obtained from Sigma Aldrich and were used without purification.

### 1.2 Cocrystal synthesis

Cocrystals were prepared by mixing equimolar quantities of halogen bond donors and acceptors in suitable solvent, most often dichloromethane (DCM). Samples of *cis*-**1** and **-2** after weighing and dissolving in a solvent were irradiated by 532 nm light to ensure ~100% *cis*-isomer content. Single crystals were obtained by slow evaporation of the solvent, while samples for thermal and Fourier-transform infrared attenuated total reflection (FTIR-ATR) spectroscopy analyses were made by quick evaporation to limit partial thermal isomerisation of *cis*-**1** and **-2**.

#### Cocrystal (*trans*-**1**)(**apy**)

10.0 mg (0.021 mmol) of *trans*-**1** was dissolved in 2.5 ml of DCM and added to a solution of 3.80 mg (0.021 mmol) of **apy** in 2.5 ml of DCM. Solution remained clear after mixing and cocrystals precipitated when nearly all solvent evaporated. The cocrystal melts with decomposition at 204°C, different from the melting points of **apy** (111 °C) and *trans*-**1** (222°C).

#### Cocrystal (*trans*-**1**)(*trans*-**bpe**)

10.0 mg (0.021 mmol) of *trans*-**1** was dissolved in 2.5 ml of DCM and added to the solution of 3.80 mg (0.021 mmol) of *trans*-1,2-bis(4-pyridyl)ethylene (*trans*-**bpe**) in 2.5 ml of DCM. Solution remained clear after mixing and cocrystals precipitated when the solvent evaporation was nearly completed. The cocrystal melts with decomposition at 209°C.

#### Cocrystal (*cis*-**1**)(**apy**)

10.0 mg (0.021 mmol) of *cis*-**1** was dissolved in 2.5 ml of DCM and added to the solution of 3.80 mg (0.021 mmol) of **apy** in 2.5 ml of DCM. Solution remained clear after mixing and cocrystals precipitated when the solvent evaporation was nearly completed. On the DSC plot, a broad exotherm between 150-180°C can be observed corresponding to thermal *cis-trans* reversion. The cocrystal melts with decomposition at 203°C.

#### Cocrystal (*cis*-**1**)(*trans*-**bpe**)

10.0 mg (0.021 mmol) of *cis*-**1** was dissolved in 2.5 ml of DCM and added to the solution of 3.80 mg (0.021 mmol) of *trans*-**bpe** in 2.5 ml of DCM. Solution remained clear after mixing and

cocrystals precipitated when the solvent evaporation was nearly completed. In the course of thermal analysis an exothermal peak between 140-170°C can be observed which corresponds to thermal cis-trans reconversion. The cocrystal then melts with decomposition at 209°C.

Cocrystal (*trans-2*)(**apy**)

10.0 mg (0.017 mmol) of *trans-2* was dissolved in 25 ml of DCM and added to the solution of 3.18 mg (0.017 mmol) of **apy** in 15 ml of DCM. Solution turned cloudy as predominantly microcrystalline product precipitated. The cocrystal melts with decomposition at 263°C.

Cocrystal (*trans-2*)(*trans-bpe*)

10.0 mg (0.017 mmol) of *trans-2* was dissolved in 25 ml of DCM and added to the solution of 3.18 mg (0.017 mmol) of *trans-bpe* in 15 ml of DCM. Solution turned cloudy as predominantly microcrystalline product precipitated. The cocrystal melts with decomposition at 271 °C

Cocrystal (*cis-2*)(**apy**)

10.0 mg (0.017 mmol) of *cis-2* was dissolved in 25 ml of DCM and added to the solution of 3.18 mg (0.017 mmol) of **apy** in 15 ml of DCM. Solution turned cloudy as predominantly microcrystalline product precipitated. The cocrystal melts with decomposition at 247 °C.

Cocrystal (*cis-2*)(*trans-bpe*)

10.0 mg (0.017 mmol) of *cis-2* was dissolved in 25 ml of DCM and added to the solution of 3.18 mg (0.017 mmol) of *trans-bpe* in 15 ml of DCM. Solution turned cloudy as predominantly microcrystalline product precipitated. The cocrystal melts with decomposition at 266 °C.

Cocrystal (*cis-2*)(*cis-bpe*)

10.0 mg (0.017 mmol) of *cis-2* was dissolved in 25 ml of DCM and added to the solution of 3.18 mg (0.017 mmol) of *cis-1,2-bis*(4-pyridyl)ethylene (*cis-2*) in 15 ml of DCM. Cocrystals precipitated when the solvent evaporation was nearly completed. Melting with decomposition was observed at 196 °C.

Cocrystal (*trans-2*)(*cis-bpe*)

10.0 mg (0.017 mmol) of *trans-2* was dissolved in 25 ml of DCM and added to the solution of 3.18 mg (0.017 mmol) of *cis-bpe* in 15 ml of DCM. Cocrystals precipitated when the solvent evaporation was nearly completed. Melts with decomposition at 200 °C.

## 2. Single crystal X-ray diffraction measurements and crystallographic summary

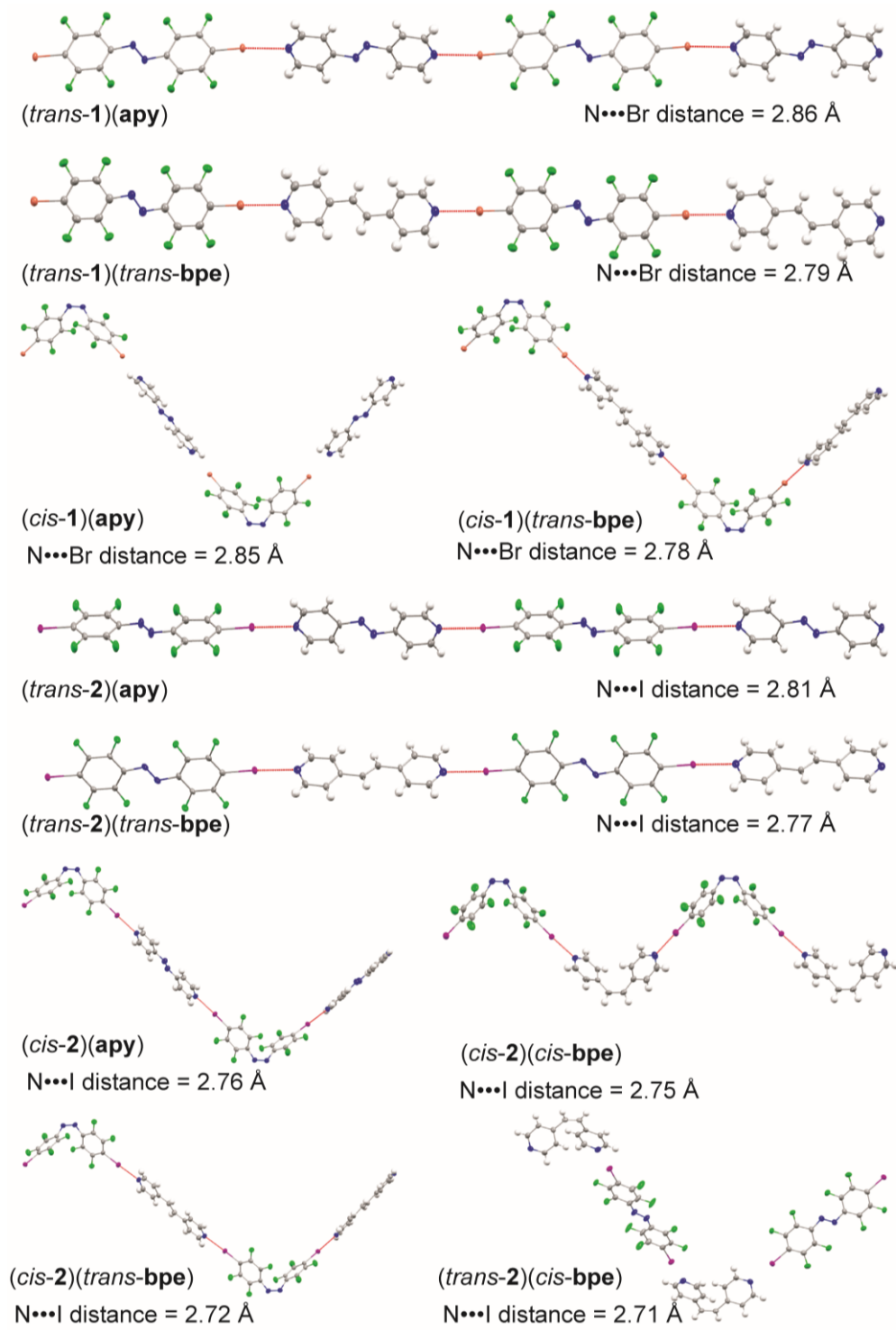


**Figure S1.** Fragments of crystal structures of prepared cocrystals, illustrating the formation of halogen-bonded chains, with representative halogen bond acceptor $\cdots$ donor distances highlighted. Thermal ellipsoids are drawn at 50% probability. Element colors: grey (carbon), blue (nitrogen), green (fluorine), purple (iodine) and brown (bromine).

X-ray single crystal diffraction data was obtained on Bruker D8 single-crystal X-ray diffractometer equipped with a MoK $\alpha$  X-ray source and a graphite monochromator. Multi-scan absorption correction (SADABS) was applied for all collected datasets. Structures were solved by direct methods and refined using SHELX-97 software.<sup>2</sup> Data summary is presented in Table S2. Crystallographic data for all prepared cocrystals has been deposited with the Cambridge Structural Database (deposition codes 984291-984300)

**Table S1.** General and crystallographic data for the prepared cocrystals.

Compound	( <i>trans</i> -1)( <i>apy</i> )	( <i>trans</i> -1)( <i>trans</i> - <i>bpe</i> )	( <i>cis</i> -1)( <i>apy</i> )	( <i>cis</i> -1)( <i>trans</i> - <i>bpe</i> )	( <i>trans</i> -2)( <i>apy</i> )	( <i>trans</i> -2)( <i>trans</i> - <i>bpe</i> )	( <i>cis</i> -2)( <i>apy</i> )	( <i>cis</i> -2)( <i>trans</i> - <i>bpe</i> )	( <i>cis</i> -2)( <i>cis</i> - <i>bpe</i> )	( <i>trans</i> -2)( <i>cis</i> - <i>bpe</i> )
Formula	C <sub>22</sub> H <sub>8</sub> Br <sub>2</sub> F <sub>8</sub> N <sub>6</sub>	C <sub>24</sub> H <sub>10</sub> Br <sub>2</sub> F <sub>8</sub> N <sub>4</sub>	C <sub>22</sub> H <sub>8</sub> Br <sub>2</sub> F <sub>8</sub> N <sub>6</sub>	C <sub>24</sub> H <sub>10</sub> Br <sub>2</sub> F <sub>8</sub> N <sub>4</sub>	C <sub>22</sub> H <sub>8</sub> F <sub>8</sub> I <sub>2</sub> N <sub>6</sub>	C <sub>24</sub> H <sub>10</sub> F <sub>8</sub> I <sub>2</sub> N <sub>4</sub>	C <sub>22</sub> H <sub>8</sub> F <sub>8</sub> I <sub>2</sub> N <sub>6</sub>	C <sub>24</sub> H <sub>10</sub> F <sub>8</sub> I <sub>2</sub> N <sub>4</sub>	C <sub>24</sub> H <sub>10</sub> F <sub>8</sub> I <sub>2</sub> N <sub>4</sub>	C <sub>24</sub> H <sub>10</sub> F <sub>8</sub> I <sub>2</sub> N <sub>4</sub>
CSD code	984297	984296	984292	984291	984299	984298	984294	984293	984295	984300
$\rho_{\text{calc}}$ (g/cm <sup>3</sup> )	1.969	1.944	1.971	1.889	2.252	2.201	2.166	2.109	2.006	2.058
Crystal system	triclinic	triclinic	monoclinic	monoclinic	triclinic	triclinic	monoclinic	monoclinic	monoclinic	monoclinic
<i>T</i> (K)	296	150	150	150	100	100	100	100	100	100
Space group	<i>P</i> -1	<i>P</i> -1	<i>C</i> 2/ <i>c</i>	<i>C</i> 2/ <i>c</i>	<i>P</i> -1	<i>P</i> -1	<i>C</i> 2/ <i>c</i>	<i>C</i> 2/ <i>c</i>	<i>C</i> 2/ <i>c</i>	<i>C</i> 2/ <i>c</i>
Unit cell parameters	<i>a</i> = 5.9081(6) Å <i>b</i> = 8.3193(9) Å <i>c</i> = 23.198(2) Å $\alpha$ = 94.956(1)° $\beta$ = 93.481(1)° $\gamma$ = 95.848(1)°	<i>a</i> = 6.083(1) Å <i>b</i> = 8.313(2) Å <i>c</i> = 12.157(2) Å $\alpha$ = 70.137(2)° $\beta$ = 84.722(2)° $\gamma$ = 79.999(2)°	<i>a</i> = 36.953(4) Å <i>b</i> = 5.2778(6) Å <i>c</i> = 11.544(1) Å $\beta$ = 90.529(1)°	<i>a</i> = 28.893(5) Å <i>b</i> = 5.236(1) Å <i>c</i> = 17.648(3) Å $\beta$ = 118.696(2)°	<i>a</i> = 5.848(2) Å <i>b</i> = 8.445(3) Å <i>c</i> = 23.132(7) Å $\alpha$ = 94.990(3)° $\beta$ = 95.779(3)° $\gamma$ = 96.339(3)°	<i>a</i> = 5.8317(6) Å <i>b</i> = 8.5364(9) Å <i>c</i> = 23.470(3) Å $\alpha$ = 95.753(1)° $\beta$ = 96.748(1)° $\gamma$ = 95.828(1)°	<i>a</i> = 28.722(4) Å <i>b</i> = 5.1901(7) Å <i>c</i> = 18.220(3) Å $\beta$ = 120.623(1)°	<i>a</i> = 29.154(5) Å <i>b</i> = 5.2244(9) Å <i>c</i> = 18.283(3) Å $\beta$ = 120.726(2)°	<i>a</i> = 40.225(5) Å <i>b</i> = 5.8436(7) Å <i>c</i> = 25.726(3) Å $\beta$ = 123.647(1)°	<i>a</i> = 11.0970(9) Å <i>b</i> = 8.2444(7) Å <i>c</i> = 26.821(2) Å $\beta$ = 91.457(1)°
Unit cell volume (Å <sup>3</sup> )	1127.2(2)	569.0(2)	2251.4(4)	2342.0(7)	1124.0(6)	1146.8(2)	2337.3(6)	2393.8(7)	5034(1)	2453.0(3)
<i>Z</i>	2	1	4	4	2	2	4	4	8	4
Data resolution (°)	26.02	26.37	26.730	27.480	26.350	28.340	28.280	28.280	27.480	28.320
Data completeness (%)	98.4	98.5	99.4	97.9	99.6	99.7	94.6	92.3	97.5	91.9
Collected/independent reflections	7322/4360	4568/2302	11741/2385	9467/2627	11989/4570	13012/5145	12549/2737	9638/2729	17313/5644	7658/2804
Data/parameters/restraints	4360/344/0	2302/172/0	2385/172/0	2627/172/0	4570/343/0	5145/343/0	2737/172/0	2729/172/0	5644/343/0	2804/172/0
<i>S</i>	0.780	1.043	1.051	1.023	1.002	0.989	1.042	1.025	1.039	1.040
<i>R</i> <sub>1</sub> [for <i>I</i> ≥ 4σ( <i>I</i> )]	0.0362	0.0238	0.0270	0.0284	0.0261	0.0315	0.0214	0.0263	0.0277	0.0224
w <i>R</i> <sub>2</sub> (for all data)	0.0676	0.0578	0.0700	0.0710	0.0575	0.0763	0.0498	0.0602	0.0656	0.0446
Largest diff. peak, hole (e <sup>-</sup> Å <sup>-3</sup> )	0.410, -0.466	0.373; -0.465	0.639; -0.351	0.373; -0.334	0.725; -0.672	1.465; -0.961	0.871; -0.363	1.280; -0.554	1.305; -0.563	0.402; -0.400

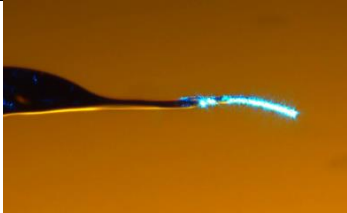
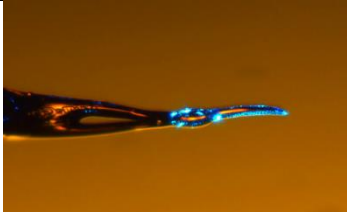
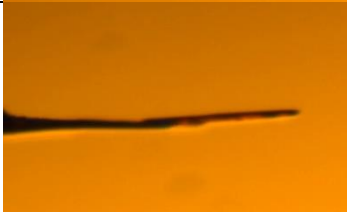
### 3. Photomechanical motion measurements

For a typical exploration of photomechanical motion, cocrystals of *cis*-1 or -2 of the approximate thickness between 10  $\mu\text{m}$  and 20  $\mu\text{m}$  were subjected to irradiation on the tip of the Mitegen® 75  $\mu\text{m}$  aperture micromounts. Irradiation was achieved by linearly polarized variable power Ar<sup>+</sup>-ion laser at 488 nm and 532 nm wavelengths and power in the range between of 5 mW/cm<sup>2</sup> and 400 mW/cm<sup>2</sup>. Photomechanical motion was recorded by an Infinity-1 CMOS microscopy camera fitted with a zoom lens.

#### 3.1 Videos and images of photomechanical crystal motion

**Video S1:** Bending of the (*cis*-2)(*cis*-bpe) cocrystal when subjected to 488 nm blue laser light at 2 mW beam power. The crystal remains stationary after the irradiation is stopped.

**Table S2.** Images of photomechanical *cis*-azobenzene cocrystals before and after irradiation

Cocrystal	Snapshot before irradiation	Snapshot after irradiation
( <i>cis</i> -2)( <i>cis</i> -bpe)		
( <i>cis</i> -2)( <i>trans</i> -bpe)		
( <i>cis</i> -1)( <i>trans</i> -bpe)		
( <i>cis</i> -2)(apy)		
( <i>cis</i> -1)(apy)		

#### 4. Summary of indexing the crystal of *(cis-2)(cis-bpe)* after irradiation

Cell indexing was performed in the basis of 747 reflections. Majority of the reflections (557 out of 747) could be fitted to two major domains<sup>3</sup>, described below:

domain 1: 420 reflections, 7.019, 7.06, 27.273 (reduced cell)

domain 2: 351 reflections, 137 exclusively, 190 unassigned

The unitcell was identical for the two domains, but rotated 2.3° about the reciprocal 0.315, 0.362, 1.000 axis and the real 0.792, 1.000, 0.220 axis

The remaining 190 reflections could be assigned to 10 domains with gradually diminishing size. All of them exhibit the same unitcell (identical to the second decimal) of *(trans-2)(cis-bpe)*.

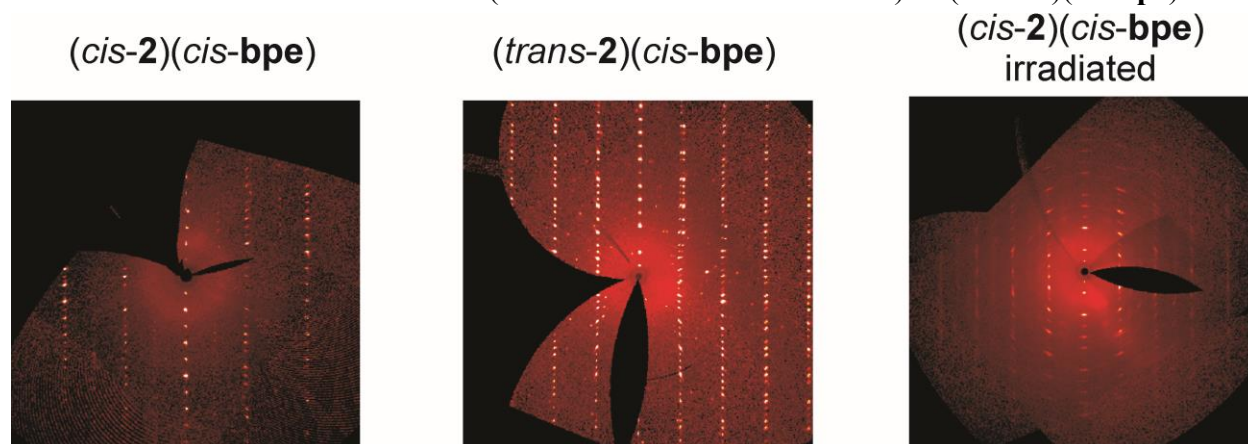


**Figure S2.** Composite diffraction images for the *0kl* diffracting plane of studied crystals. Irradiation of the cocrystal (right image) was performed by 488 nm laser light for 10 hours at 20 mW/cm<sup>2</sup>

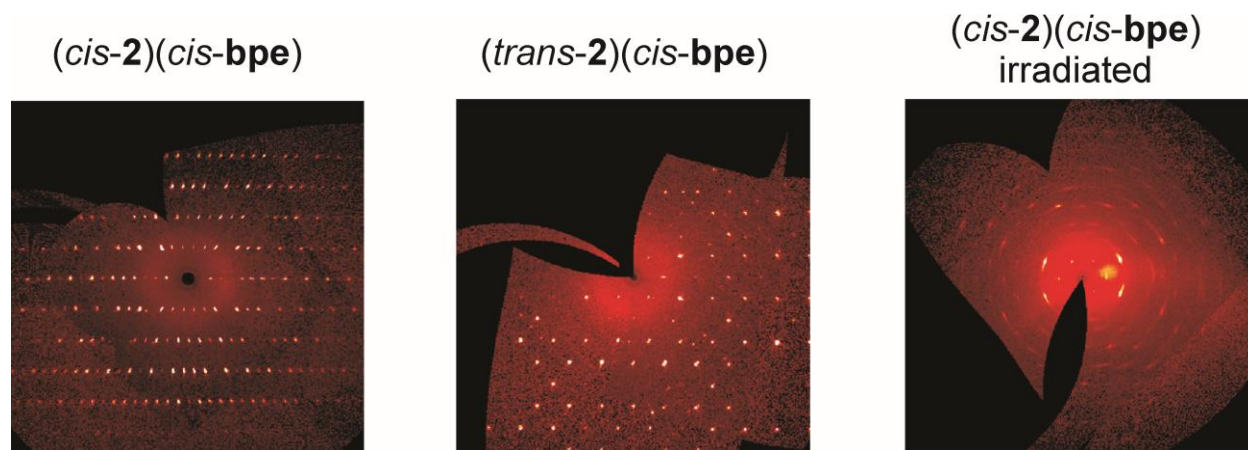
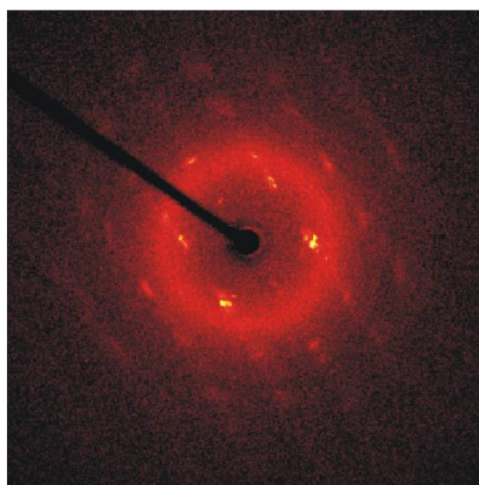
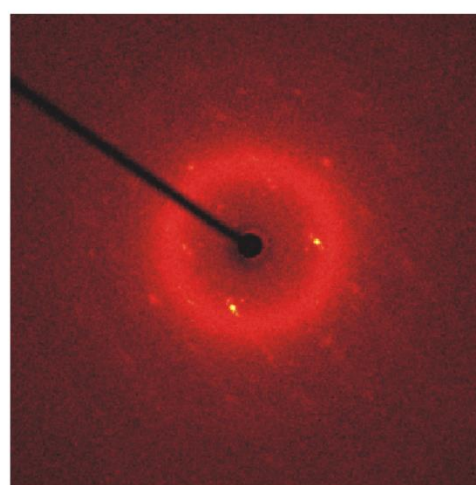


**Figure S3.** Diffraction images for the *hk0* diffracting plane of studied crystals. Irradiation of the cocrystal (right image) was performed using 488 nm laser light for 10 hours at 20 mW/cm<sup>2</sup>.

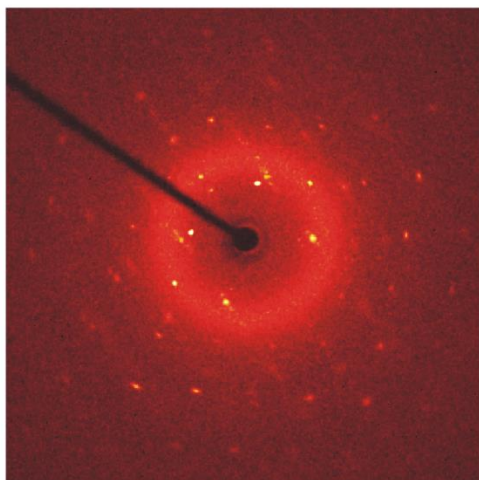
(a) an irradiated co-crystal  
usual settings



(b) a co-crystal irradiated  
with laser rotated by 90°



(c) co-crystal irradiated with  
linearly polarized light



(d) co-crystal irradiated with  
circularly polarized light

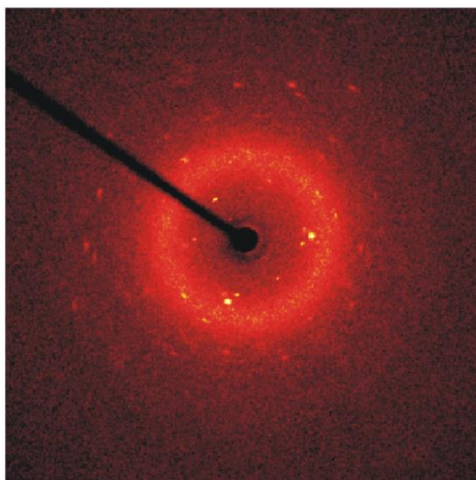


**Figure S4.** Diffraction images taken for identically oriented single crystals of *(cis-2)(cis-bpe)* after irradiation under different conditions: (a) standard experiment geometry; (b) irradiation with the laser rotated 90° around the sample; (c) irradiation using linearly polarized light and (d) irradiation using circularly polarized light. All the diffraction images are very similar, indicating that the orientation of the crystalline product phase (*trans-2)(cis-bpe)* is identical and that the photochemical isomerisation is topotactic.

## 5. Powder X-ray diffraction data

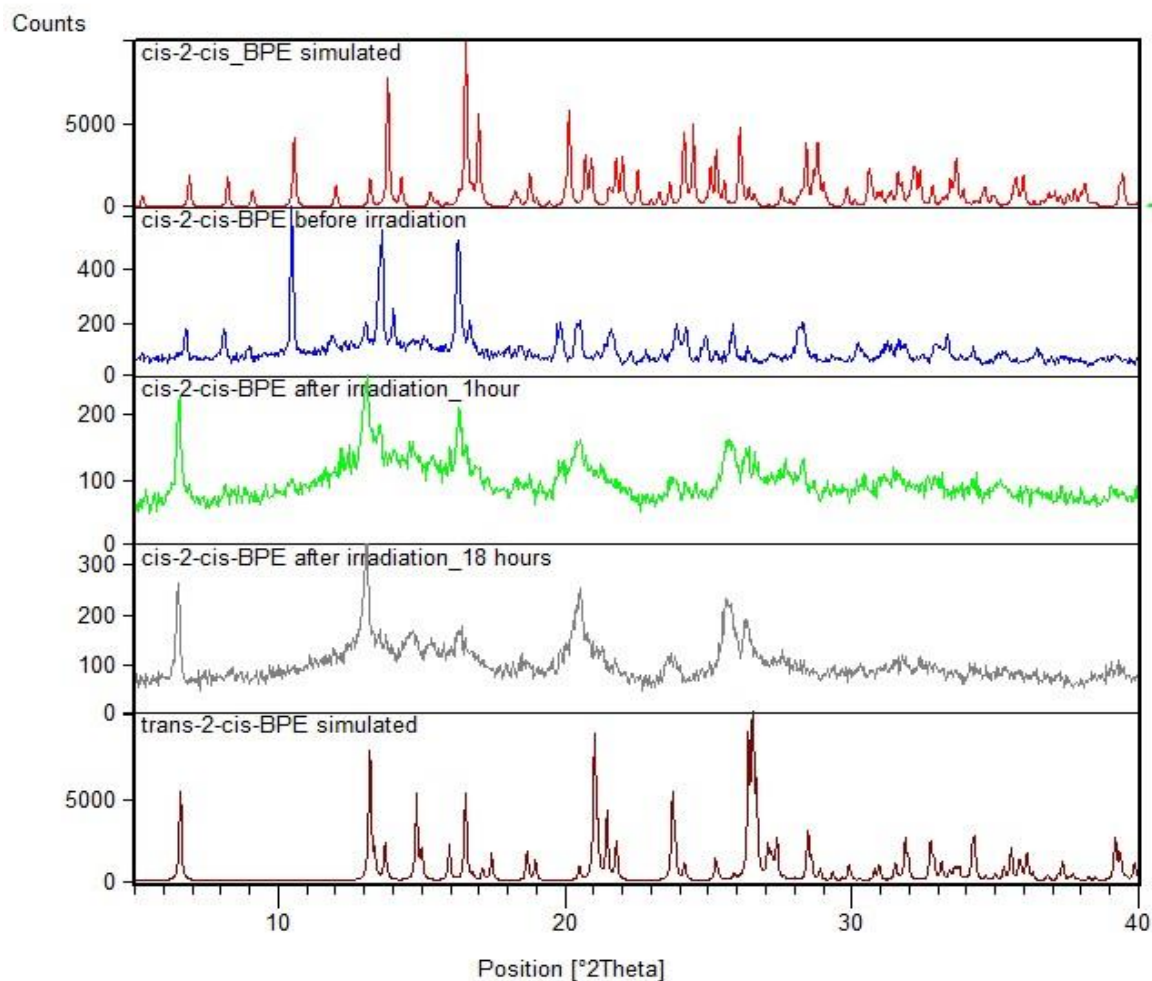


**Figure S5.** Selected powder X-ray diffraction patterns. From top to bottom: simulated pattern of (*cis-2*)(*cis-bpe*); experimental pattern for a sample of (*cis-2*)(*cis-bpe*) before irradiation; experimental pattern for (*cis-2*)(*cis-bpe*) after irradiation for 1 hour; experimental pattern for a sample of (*cis-2*)(*cis-bpe*) after irradiation for 20 hours and simulated pattern for (*trans-2*)(*cis-bpe*). The comparison of the PXRD patterns shows that the product of extended irradiation of crystalline (*cis-2*)(*cis-bpe*) is the (*trans-2*)(*cis-bpe*) crystal. The broadness of the (*trans-2*)(*cis-bpe*) X-ray reflections after irradiation is consistent with the presence of an amorphous phase indicated by *in situ* single crystal X-ray diffraction measurements.

## 6. Thermal analysis data

**Video S2.** Heating of a crystal of *cis-1* on the hot stage microscope at a rate of 10 °C/min. Crystal melts, isomerisation into the *trans*-form takes place, followed by crystallisation and subsequent melting again at a temperature corresponding to the melting point of *trans-1*. The relevant DSC thermogram is provided in Figure S6.

**Video S3.** Heating of the (*cis-2*)(*cis-bpe*) cocrystal on the hot stage microscope at a rate of 10 °C/min. The crystal does not melt, but undergoes a colour change, first visible around 130 °C, which is indicative of a solid-state *cis-trans* isomerisation. This is followed by chemical decomposition.

**Video S4.** Heating of the (*cis-1*)(*trans-bpe*) cocrystal on the hot stage microscope at a rate of 10 °C/min. similar to the cocrystal (*cis-2*)(*cis-bpe*) (Video S3) the crystal does not melt, but undergoes a colour change indicative of a solid-state *cis-trans* isomerisation.

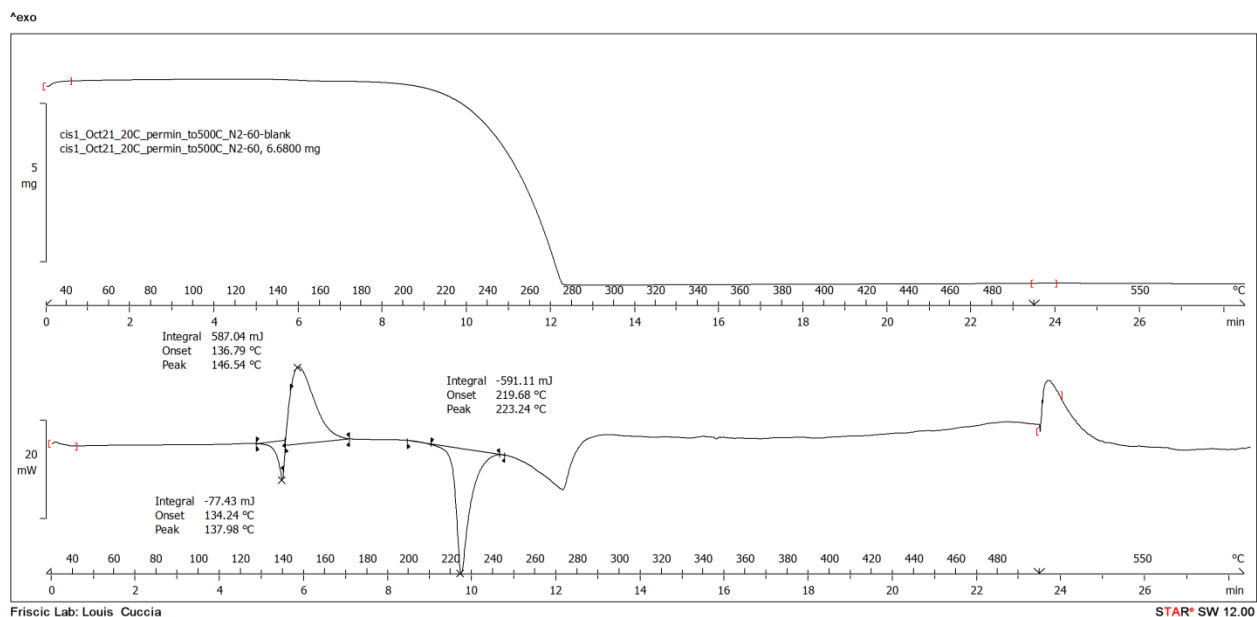


**Figure S6.** TGA (top) and DSC (bottom) thermograms of *cis-1*.

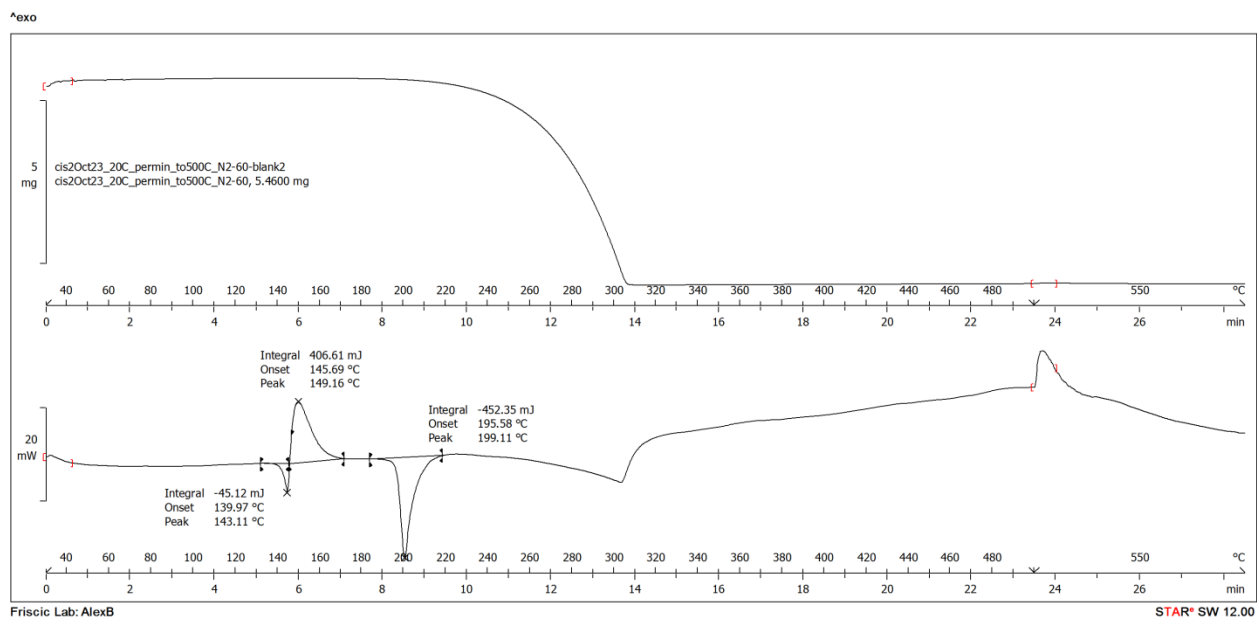


**Figure S7.** TGA (top) and DSC (bottom) thermograms of *cis-2*.

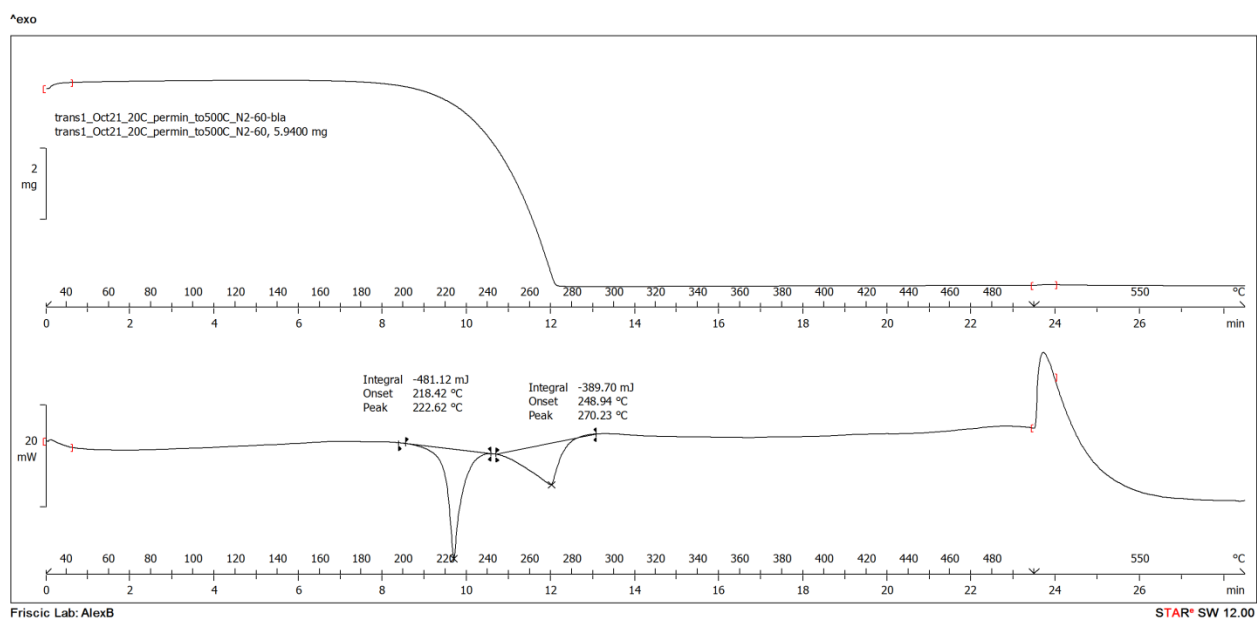


**Figure S8.** TGA (top) and DSC (bottom) thermograms of *trans-1*.

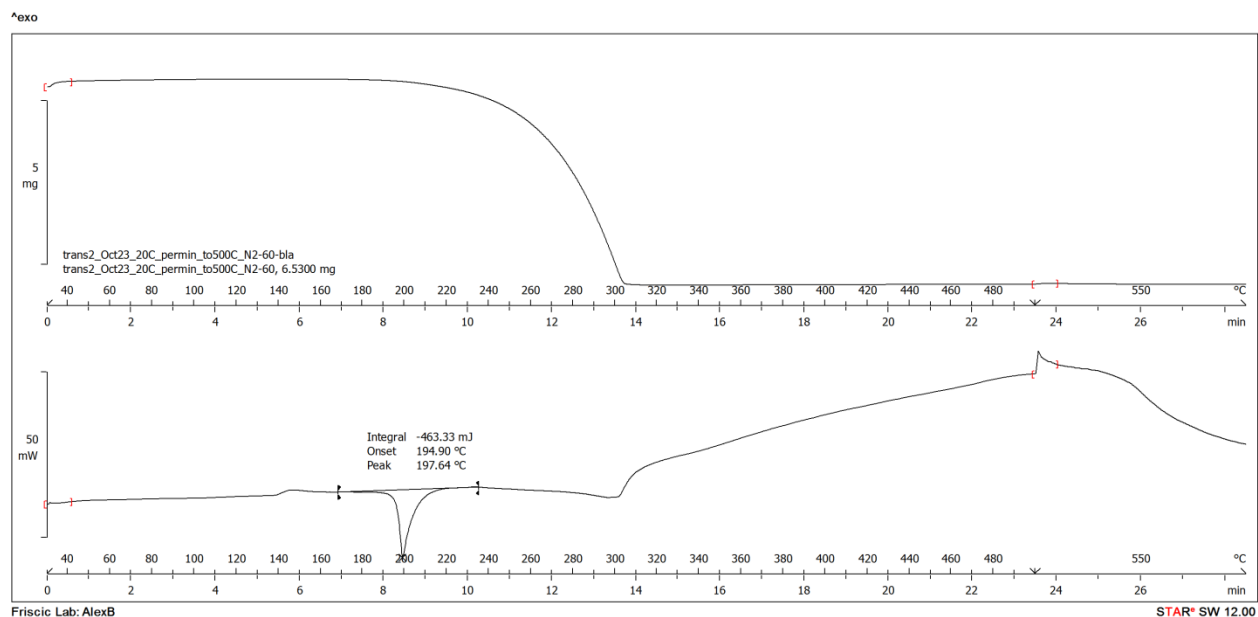


Figure S9. TGA (top) and DSC (bottom) thermograms of *trans-2*.

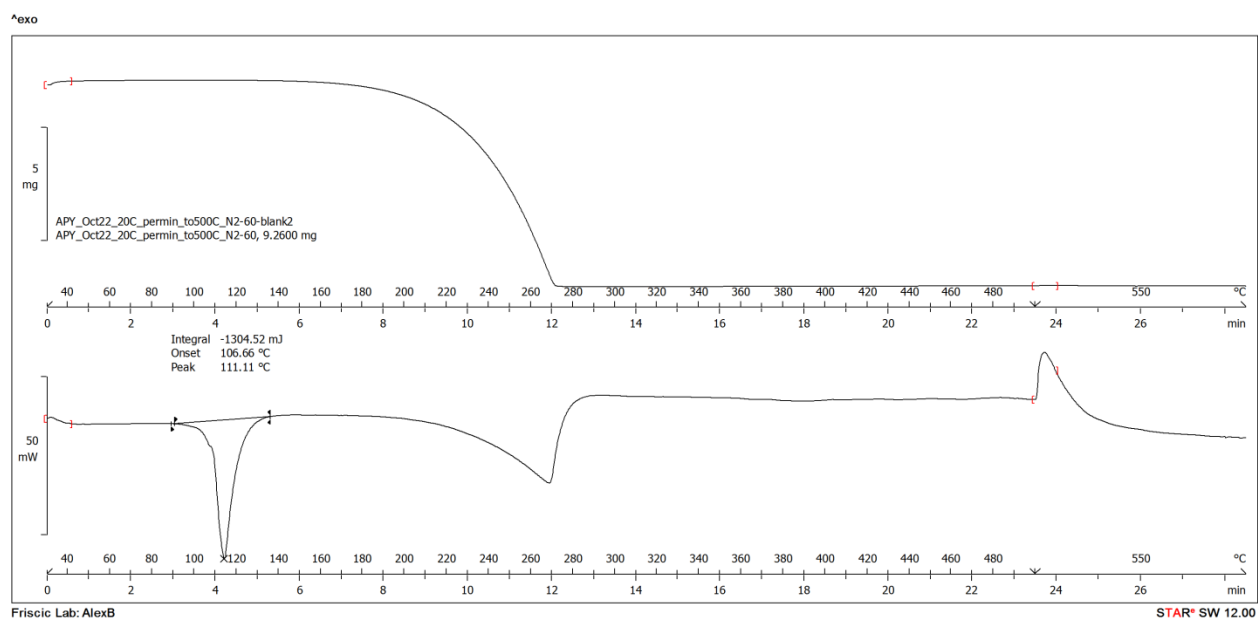


Figure S10. TGA (top) and DSC (bottom) thermograms of azopyridine (**apy**).

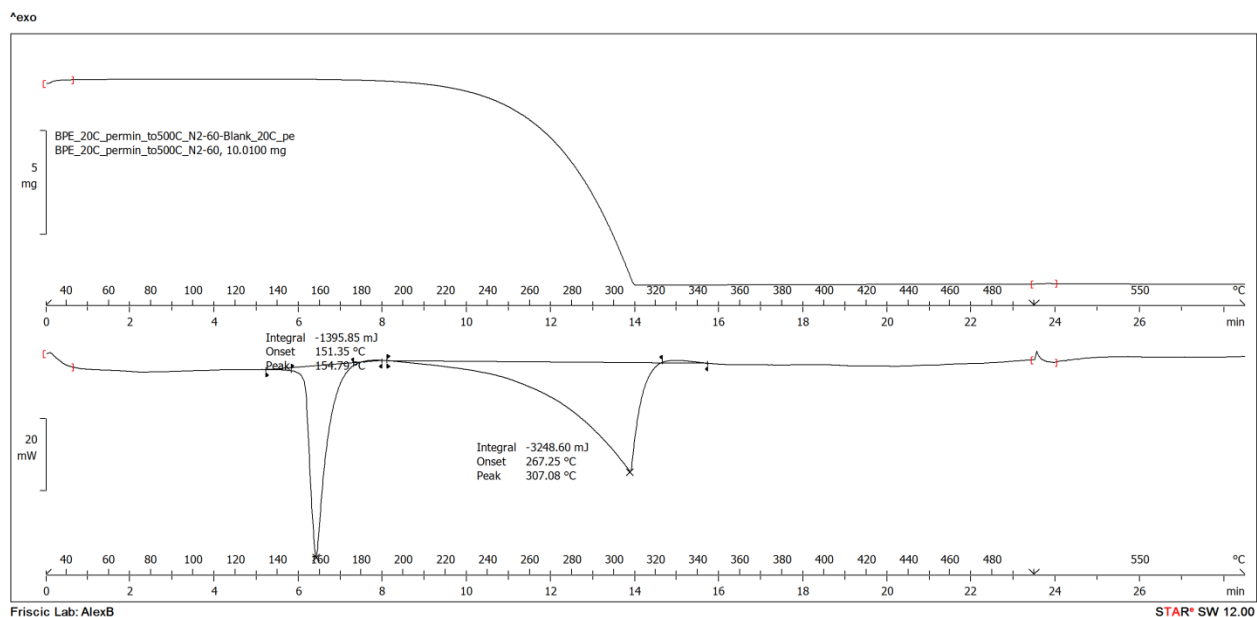


Figure S11. TGA (top) and DSC (bottom) thermograms of *trans*-bpe.

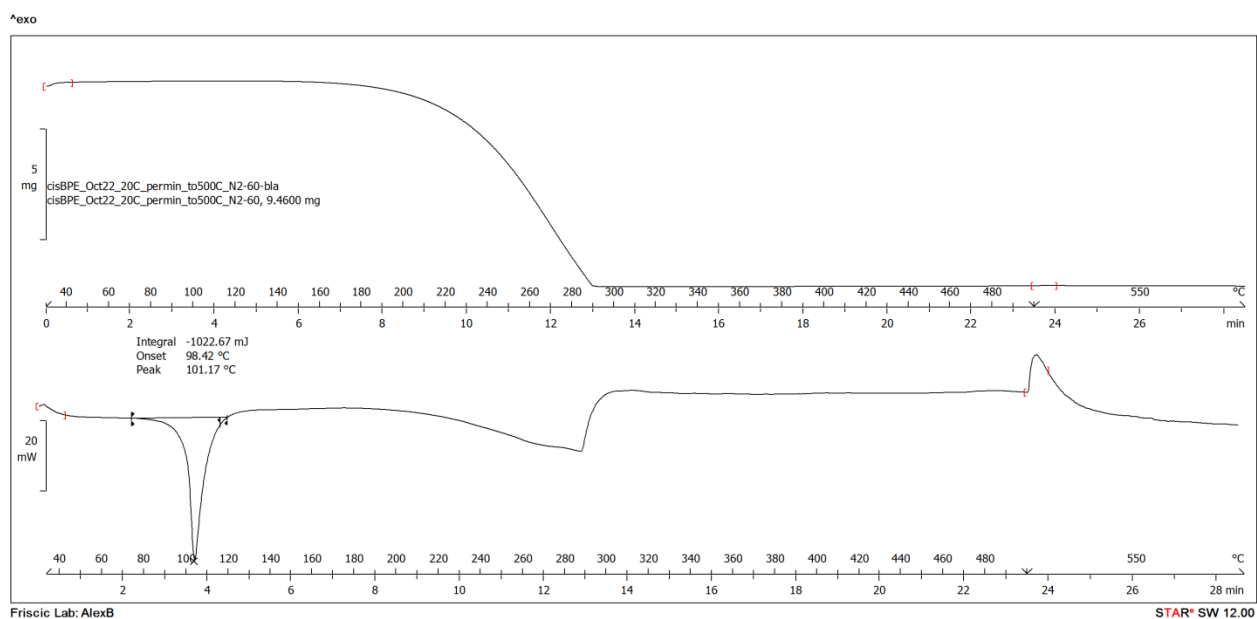
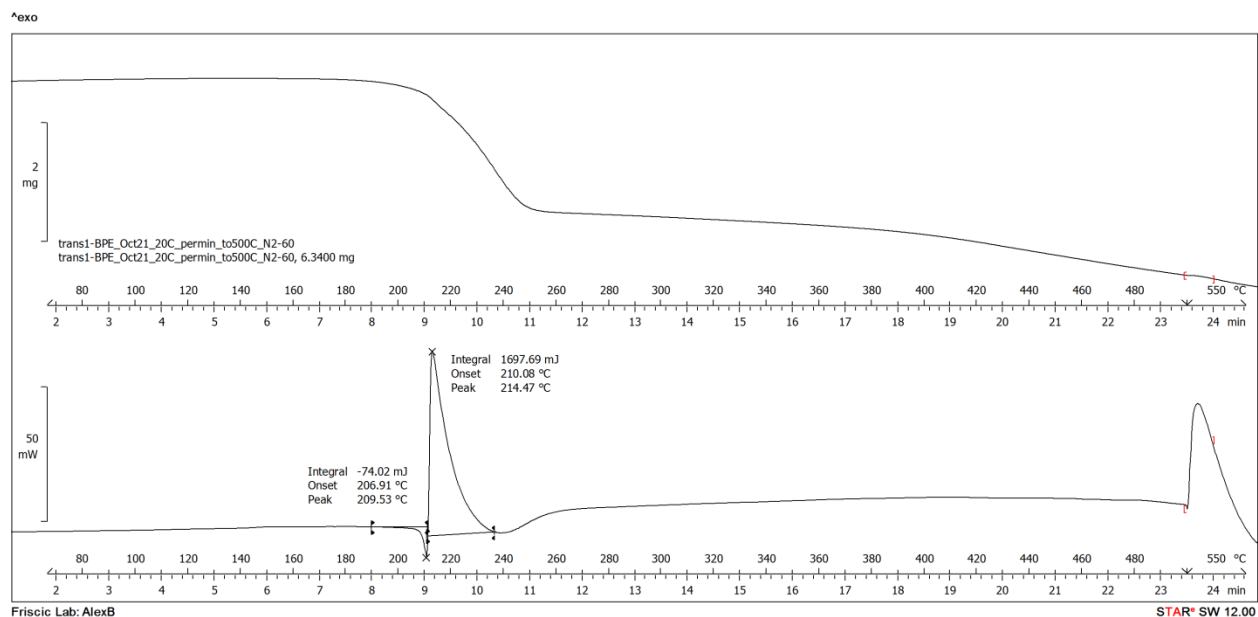
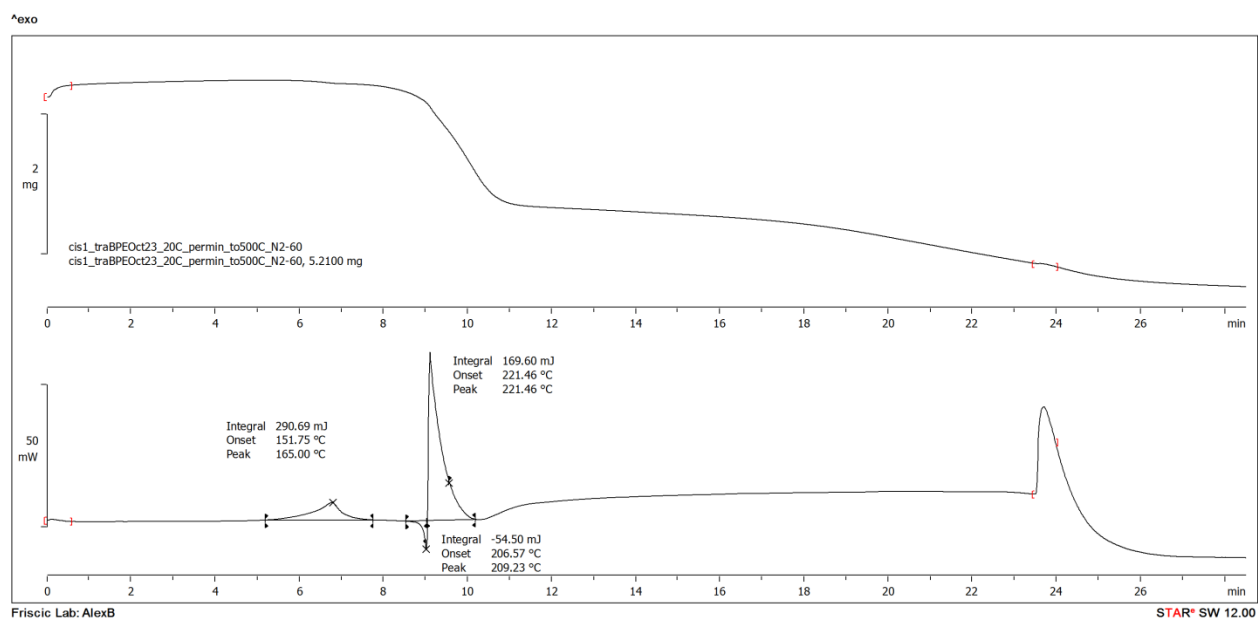


Figure S12. TGA (top) and DSC (bottom) thermograms of *cis*-bpe.



**Figure S13.** TGA (top) and DSC (bottom) thermograms of the *(trans-1)(trans-bpe)* cocrystal.



**Figure S14.** TGA (top) and DSC (bottom) thermograms of the *(cis-1)(trans-bpe)* cocrystal.

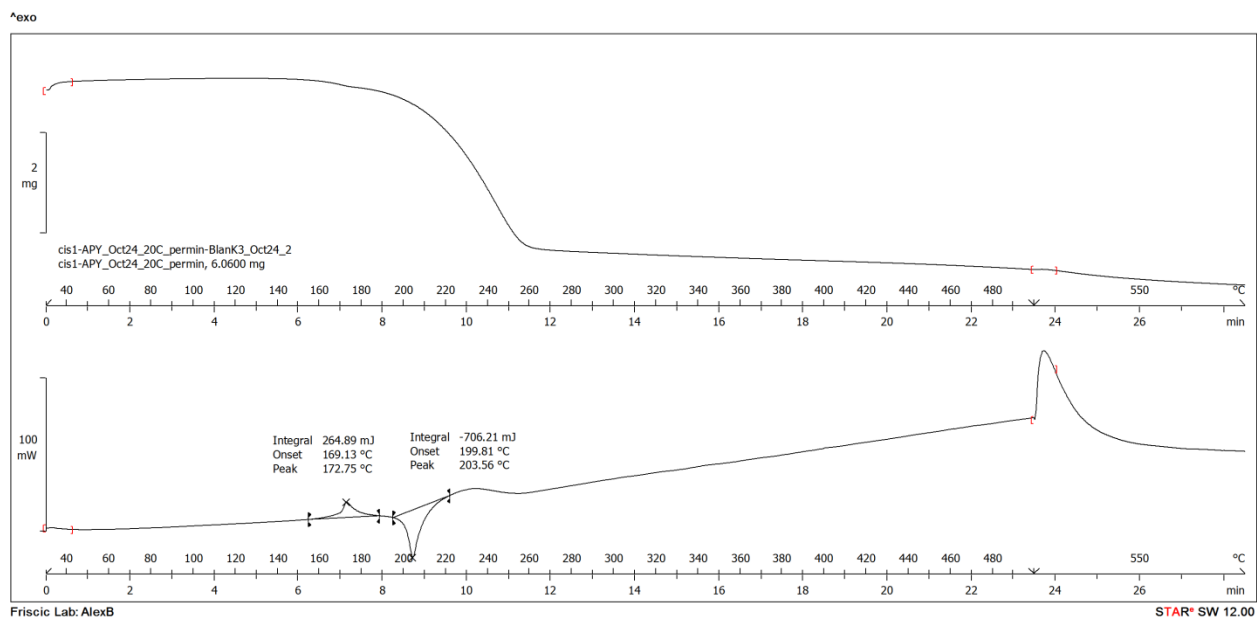


**Figure S15.** TGA (top) and DSC (bottom) thermograms of the (*cis-1*)(apy) cocrystal.

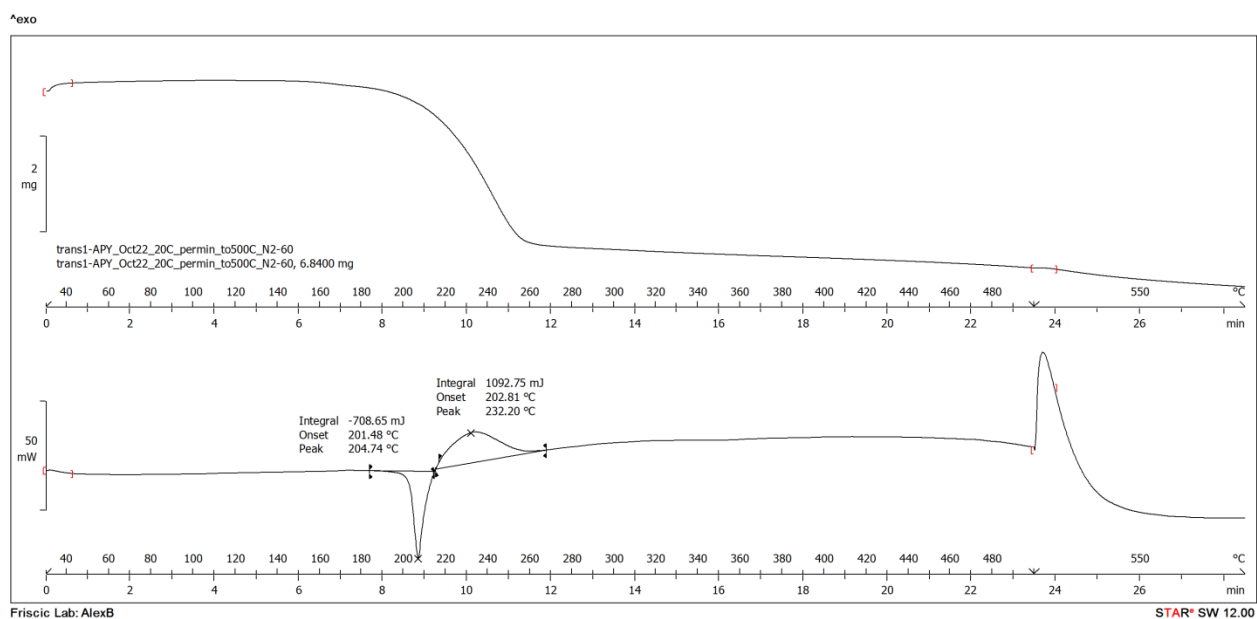


**Figure S16.** TGA (top) and DSC (bottom) thermograms of (*trans-1*)(apy).

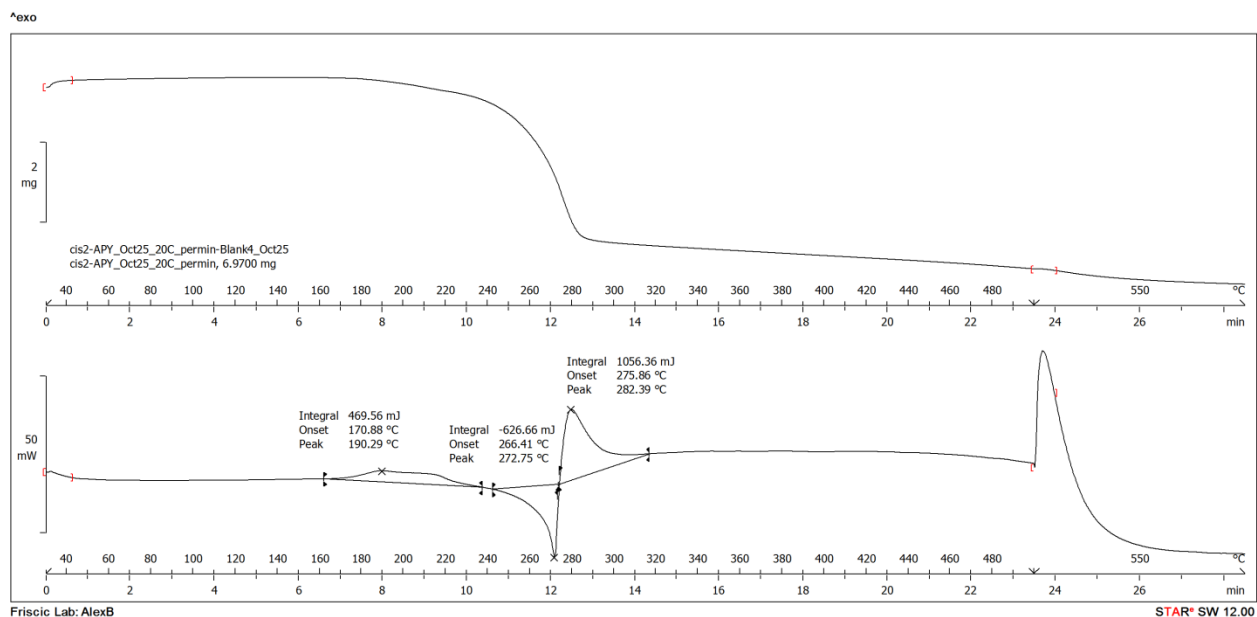


**Figure S17.** TGA (top) and DSC (bottom) thermograms of the *(cis-2)(apy)* cocrystal.

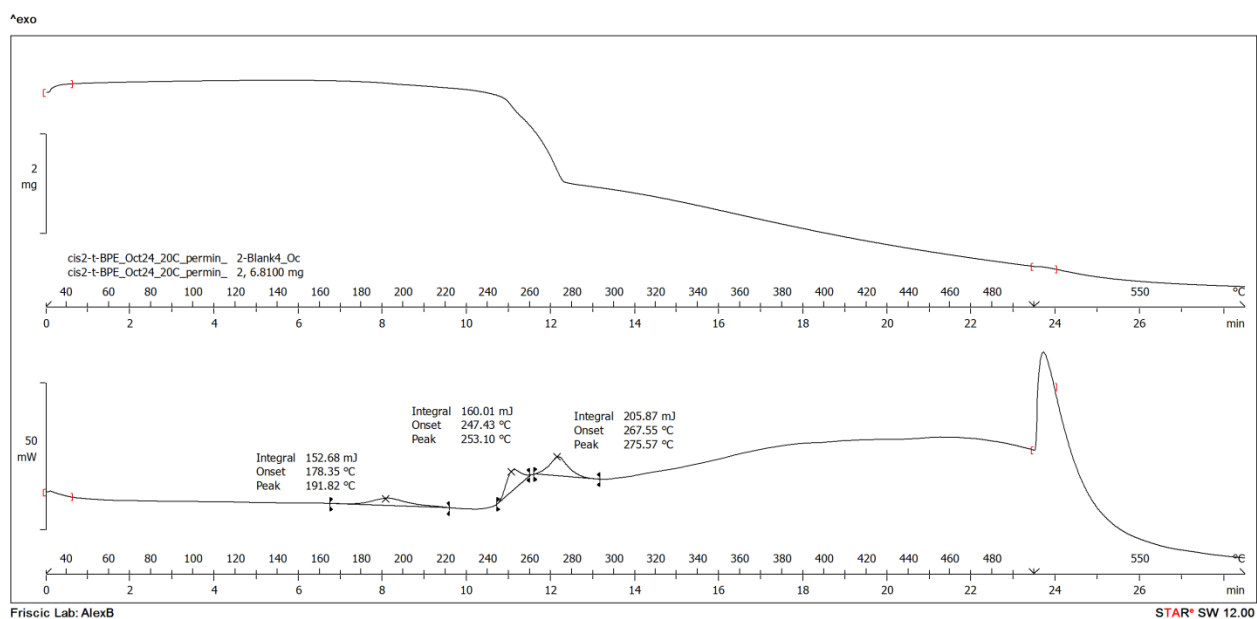


**Figure S18.** TGA (top) and DSC (bottom) thermograms of the *(cis-2)(trans-bpe)* cocrystal.

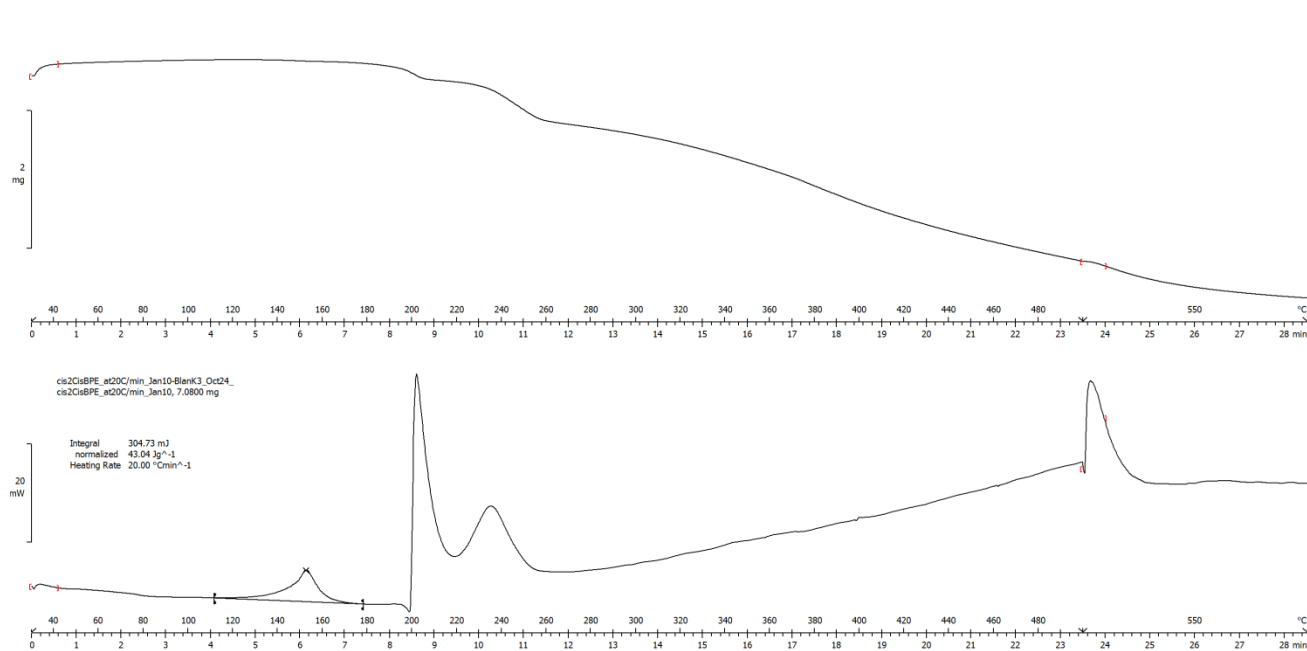


**Figure S19.** TGA (top) and DSC (bottom) thermograms of *(cis-2)(cis-bpe)* cocrystal.

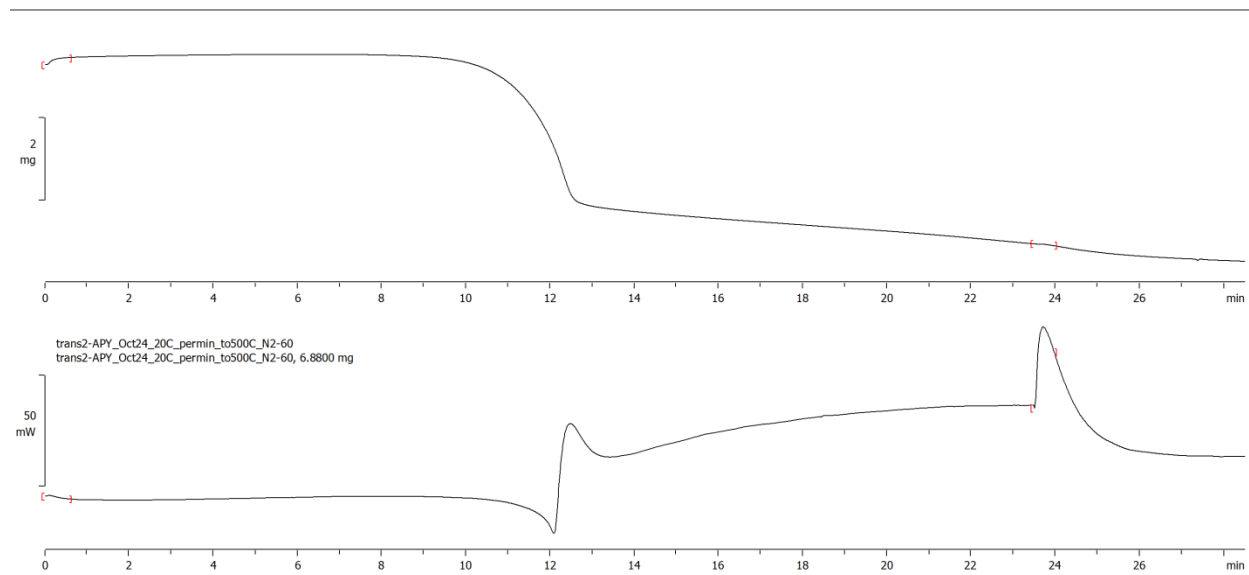


**Figure S20.** TGA (top) and DSC (bottom) thermograms of *(trans-2)(apy)* cocrystal.

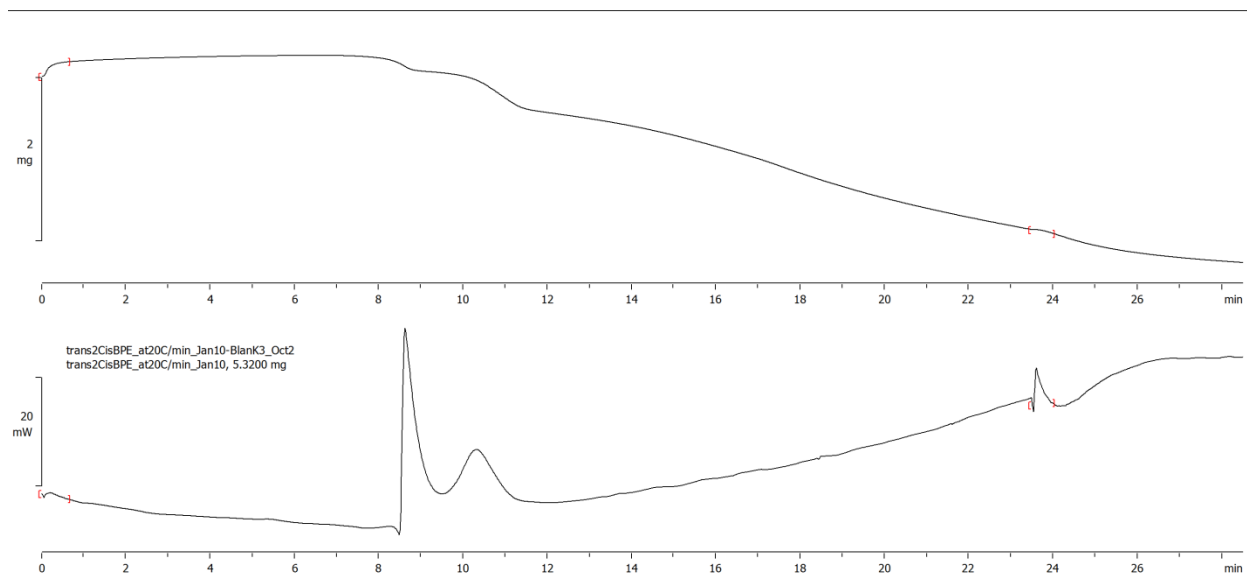


Figure S21. TGA (top) and DSC (bottom) thermograms of (*trans-2*)(*cis-bpe*) cocrystal.

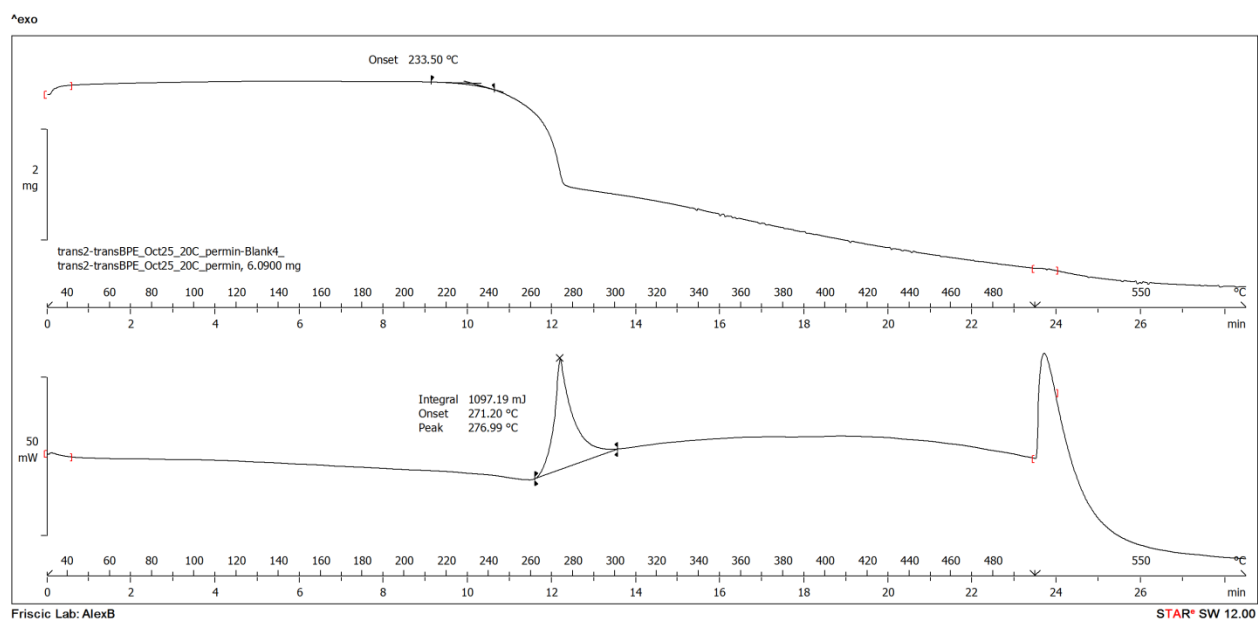
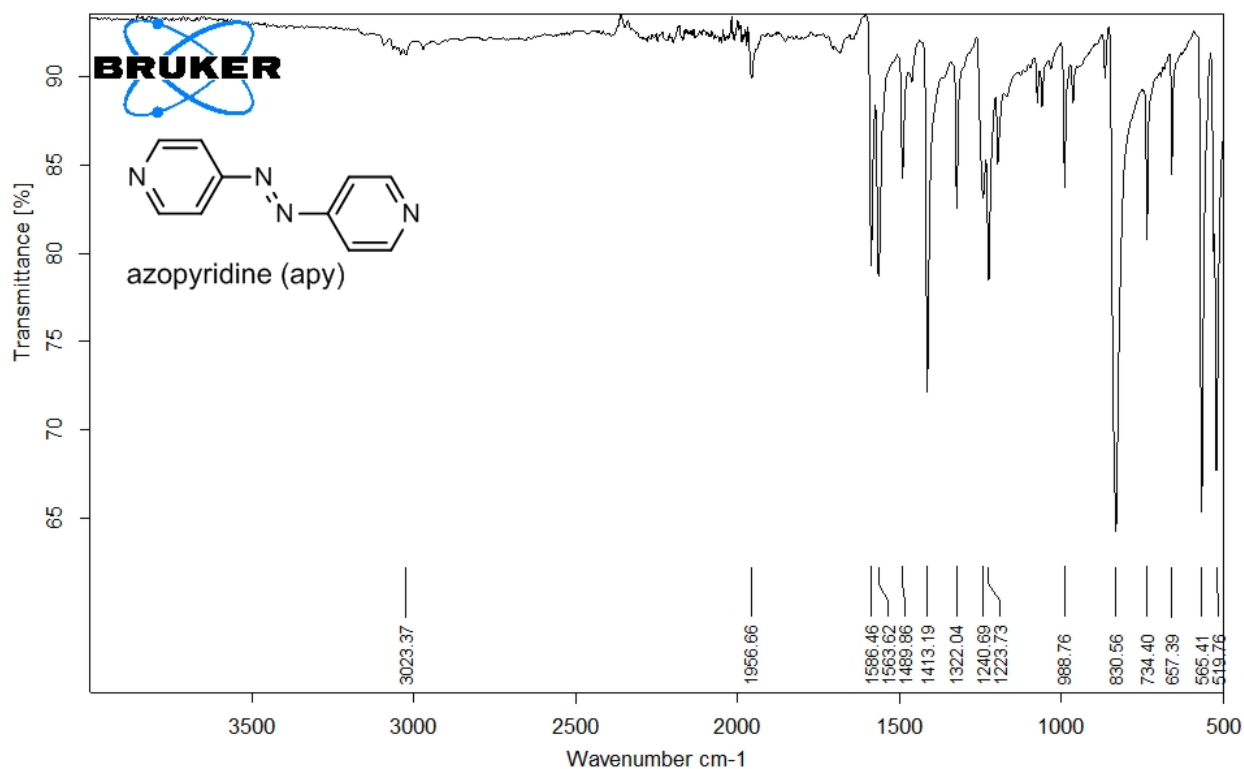


Figure S22. TGA (top) and DSC (bottom) thermograms of (*trans-2*)(*trans-bpe*) cocrystal.

## 7. Vibrational analysis data

Fourier-transform infrared attenuated total reflection (FTIR-ATR) spectra were obtained using Nicolet 6700 FTIR spectrometer and were analyzed with Bruker OPUS software, version 7.2.



**Figure S23.** FTIR-ATR spectrum of azopyridine (apy).

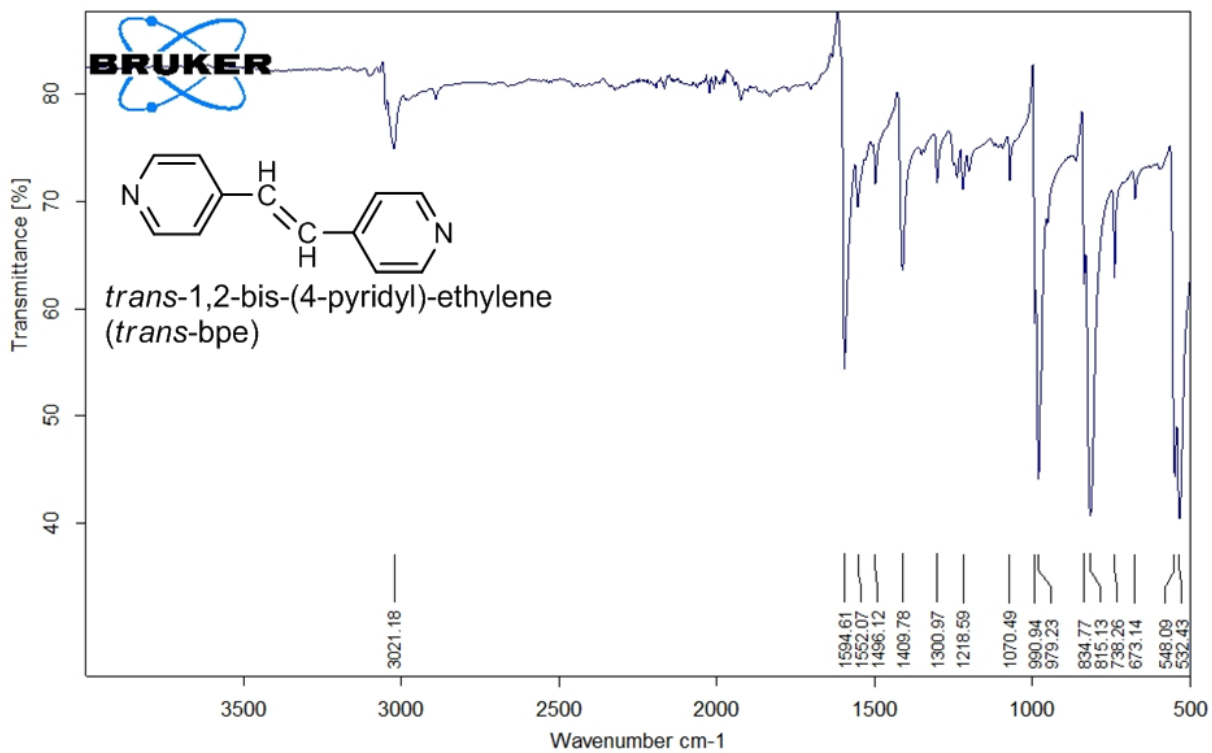


**Figure S24.** FTIR-ATR spectrum of *trans*-bpe.

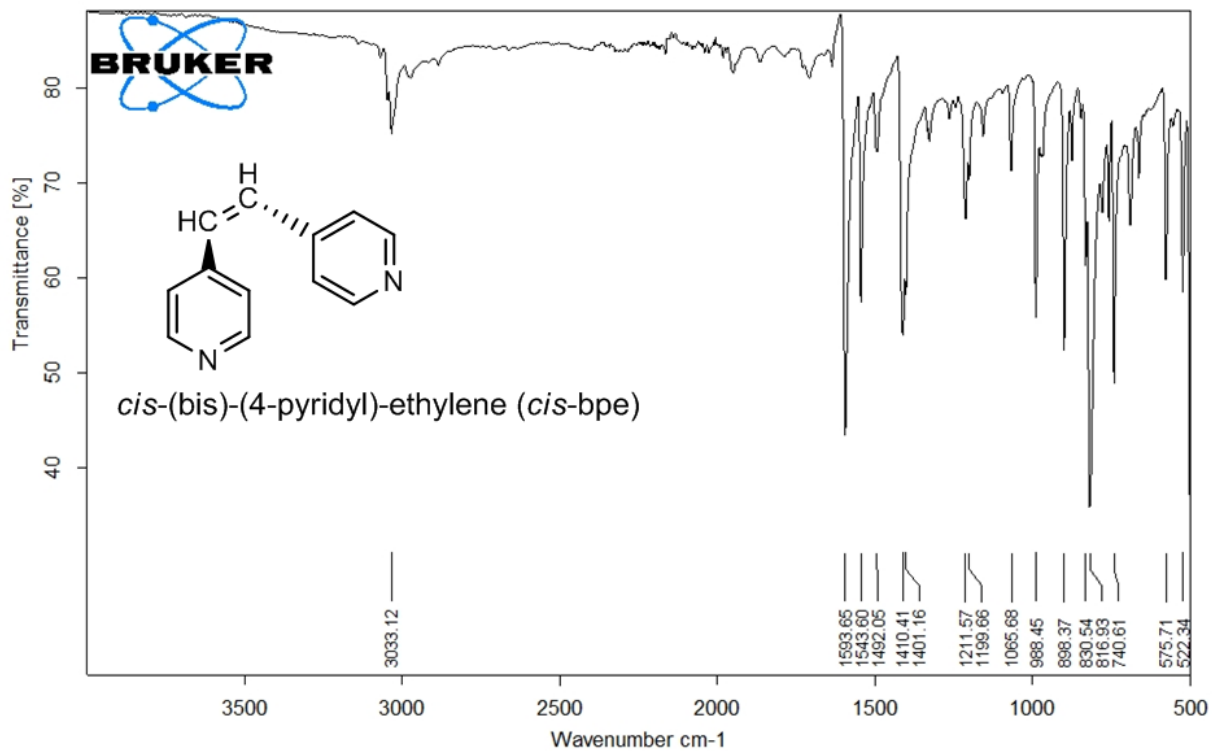


**Figure S25.** FTIR-ATR spectrum of *cis*-bpe.

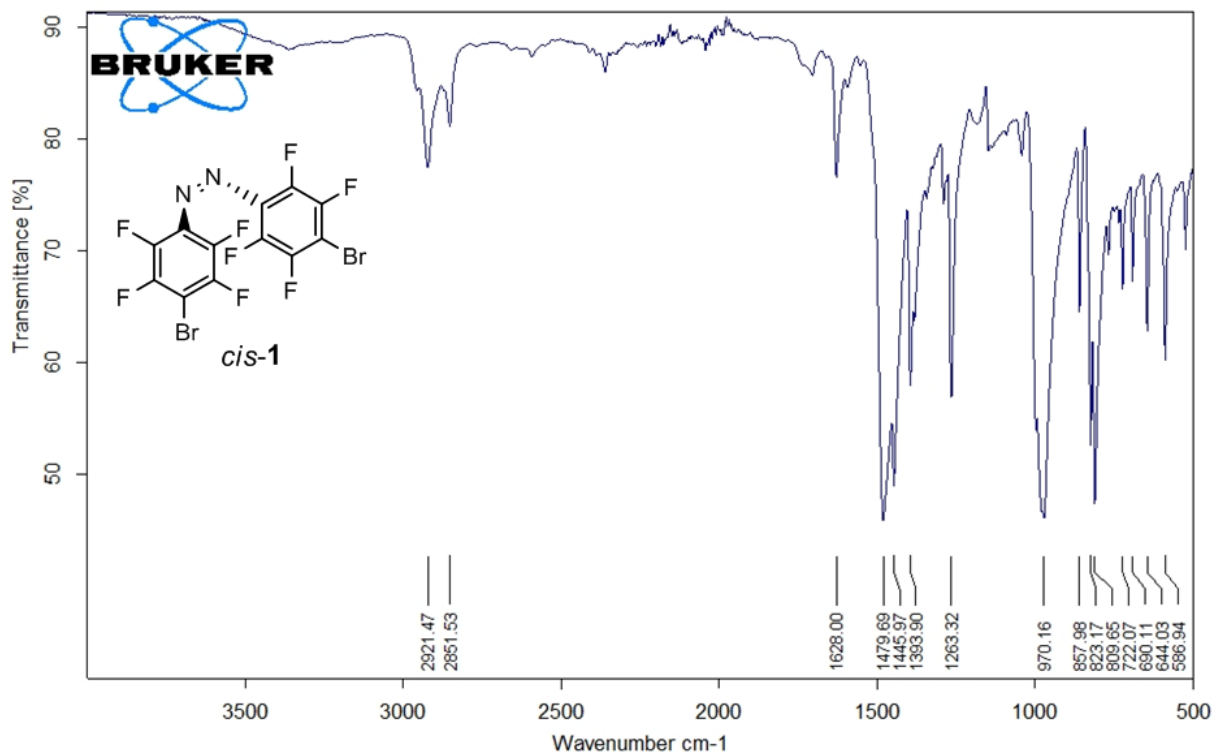


Figure S26. FTIR-ATR spectrum of *cis-1*.

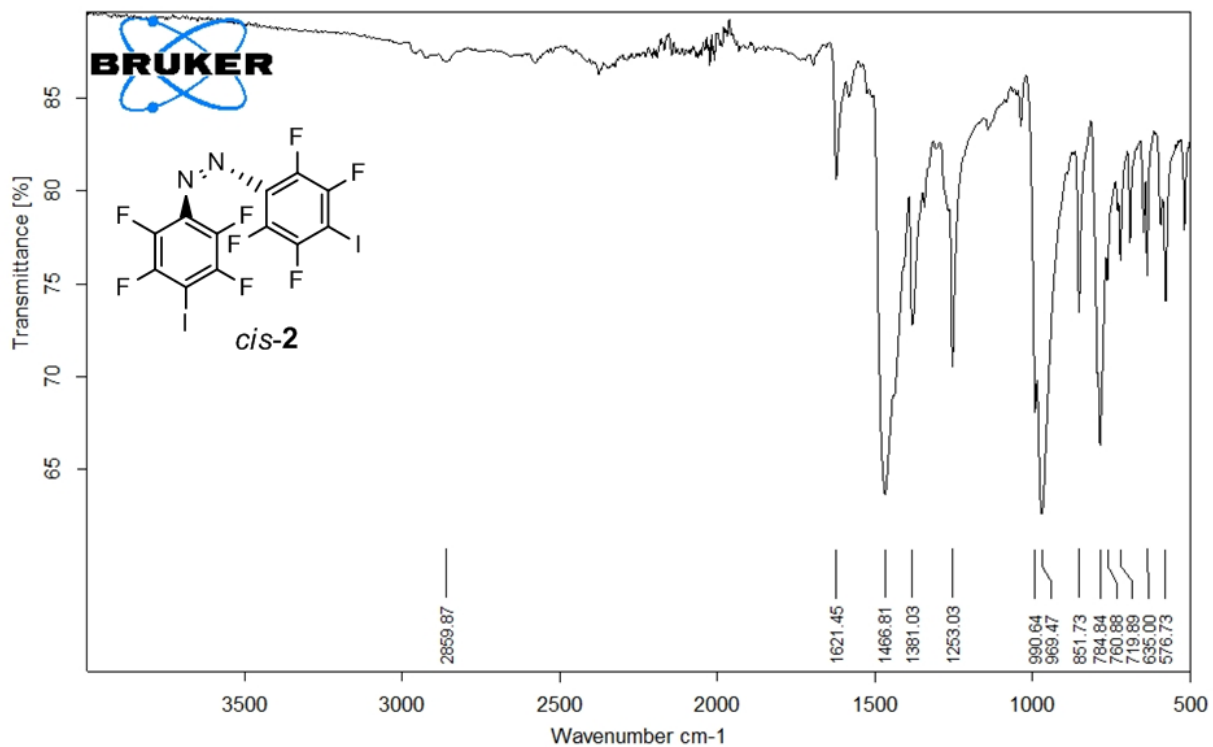


Figure S27. FTIR-ATR spectrum of *cis-2*.

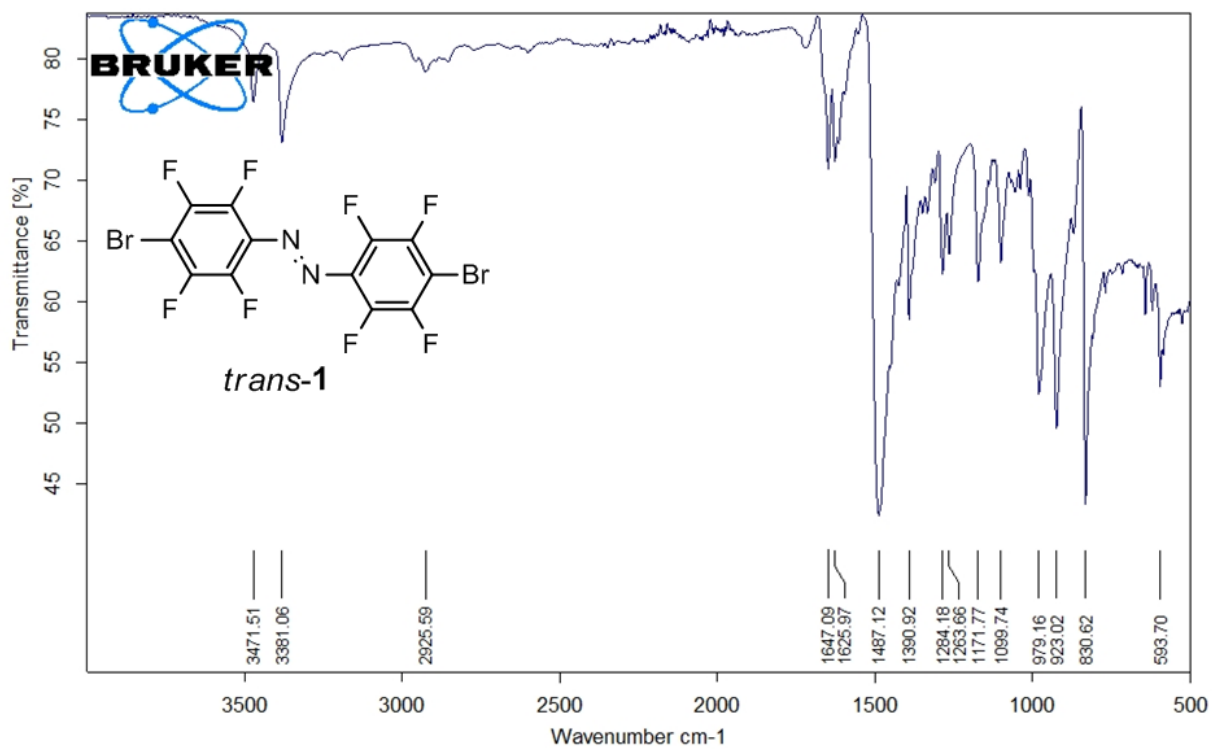


Figure S28. FTIR-ATR spectrum of *trans-1*.

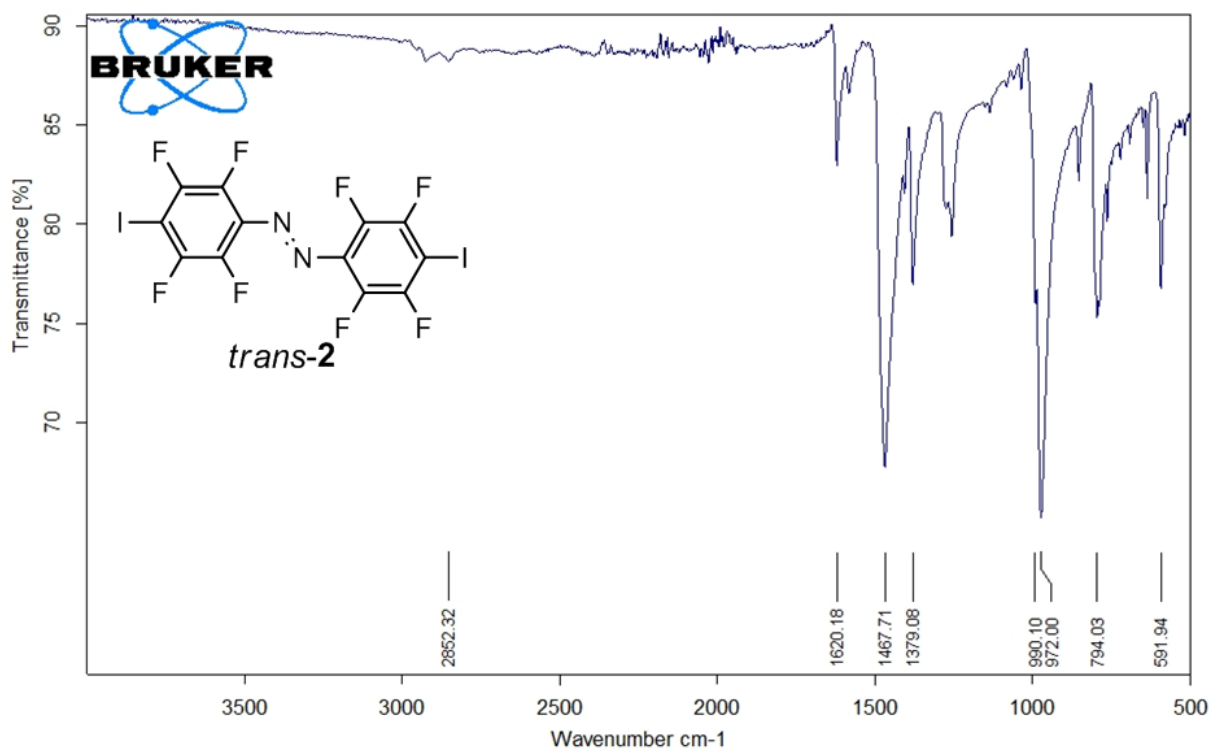


Figure S29. FTIR-ATR spectrum of *trans-2*.

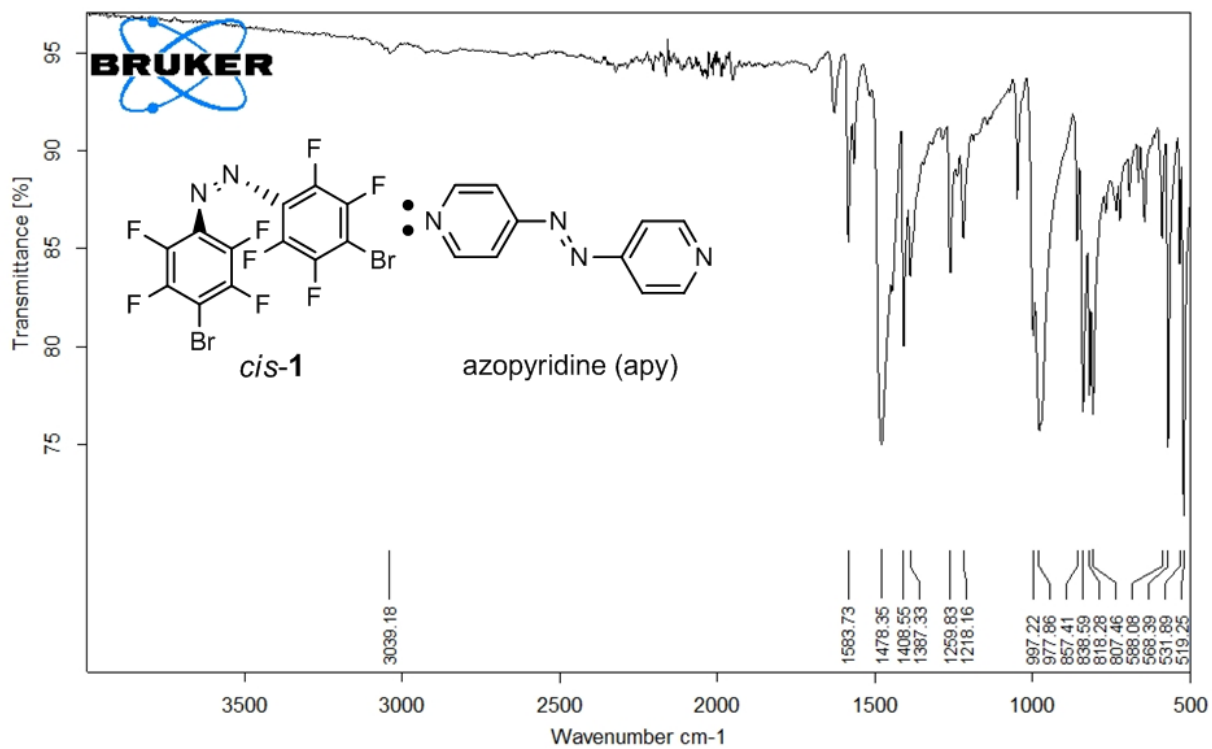


Figure S30. FTIR-ATR spectrum of *(cis-1)(apy)*.

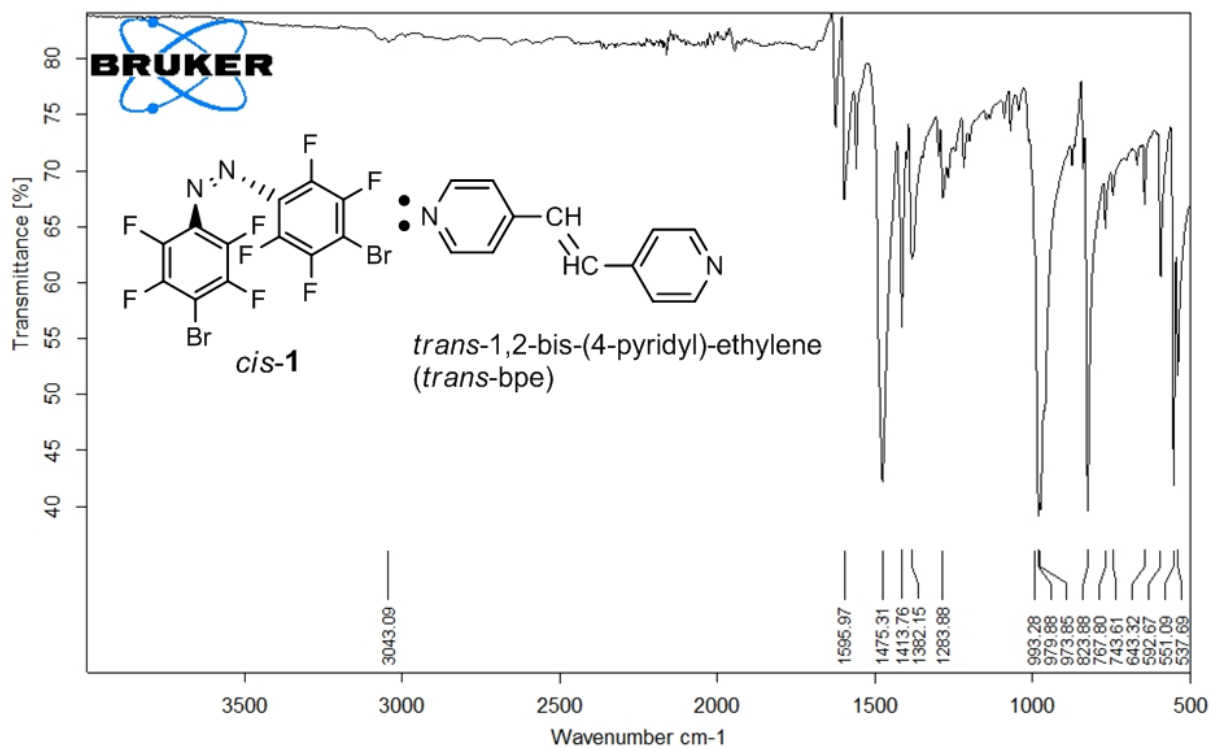


Figure S31. FTIR-ATR spectrum of *(cis-1)(trans-bpe)*.

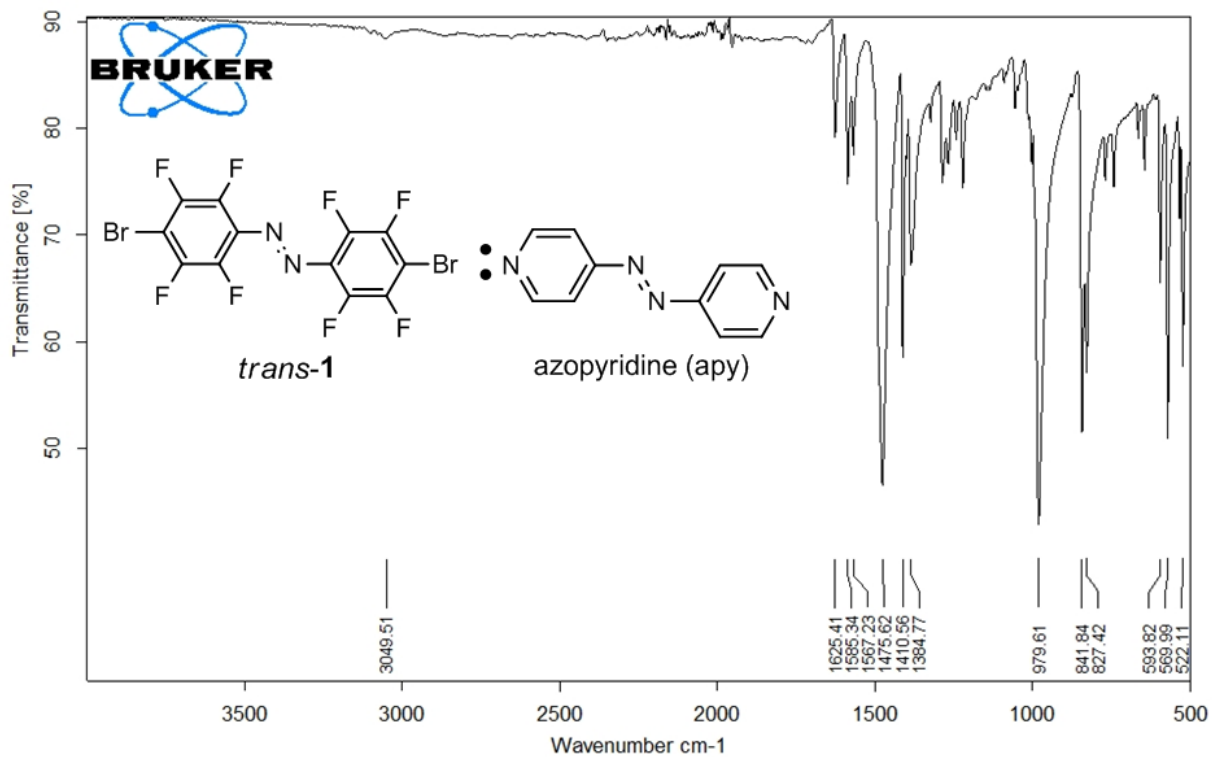


Figure S32. FTIR-ATR spectrum of (*trans-1*)(apy).

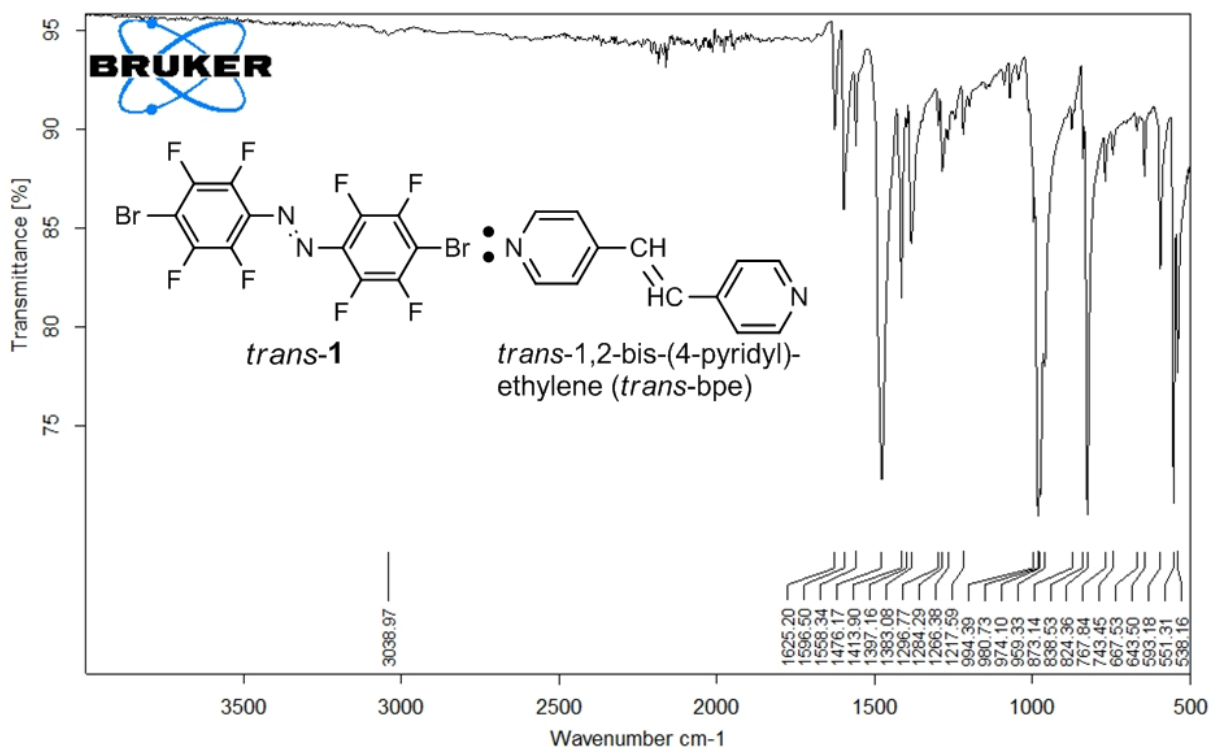


Figure S33. FTIR-ATR spectrum of (*trans-1*)(*trans-bpe*).

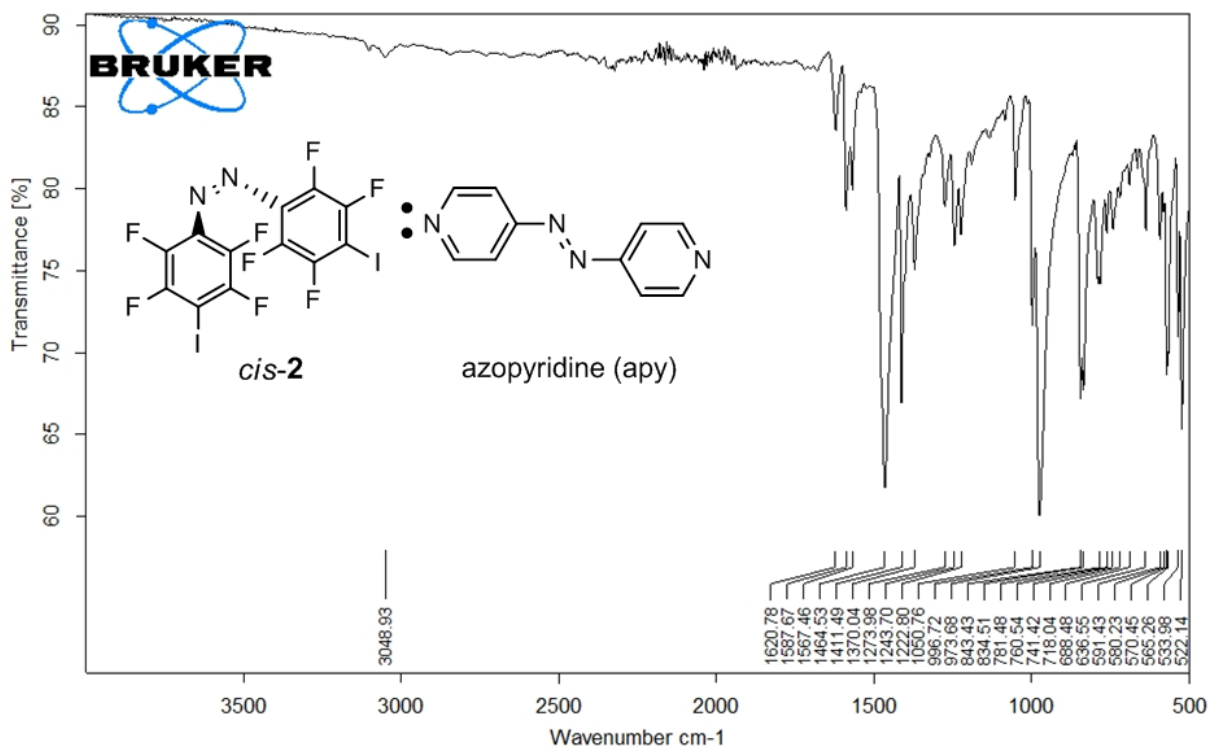


Figure S34. FTIR-ATR spectrum of (*cis-2*)(apy).

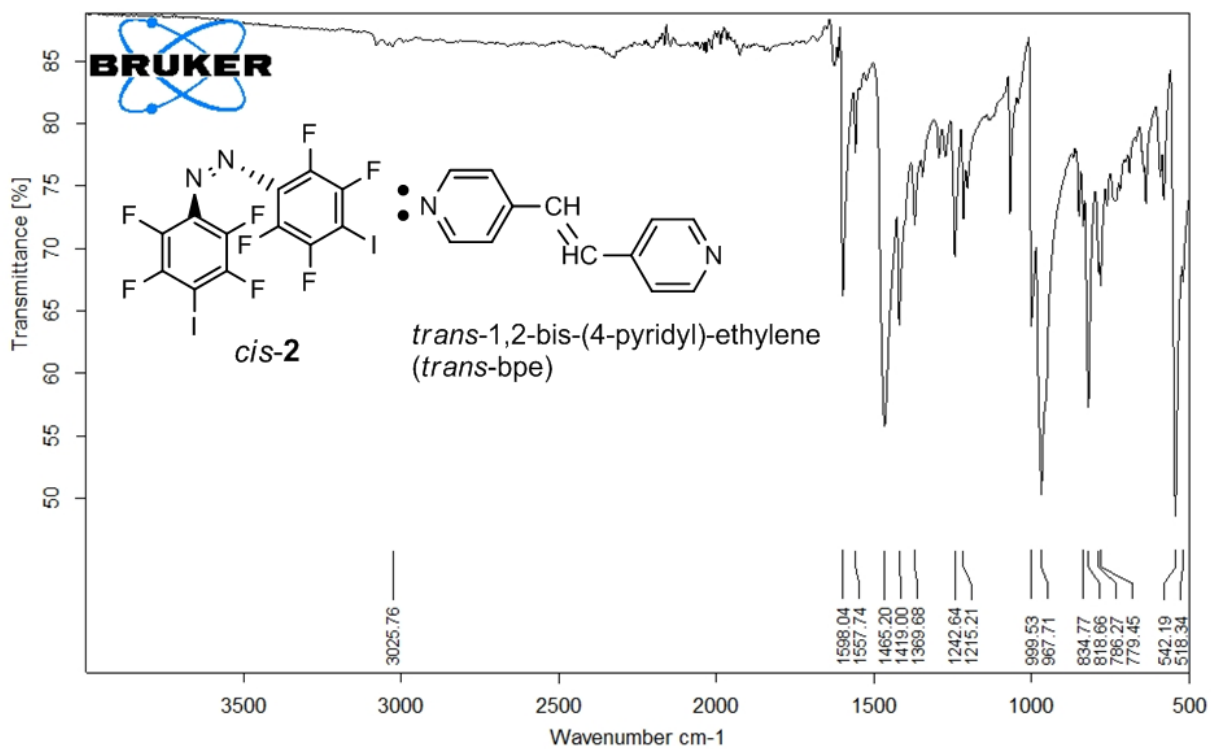


Figure S35. FTIR-ATR spectrum of (*cis-2*)(*trans-bpe*).

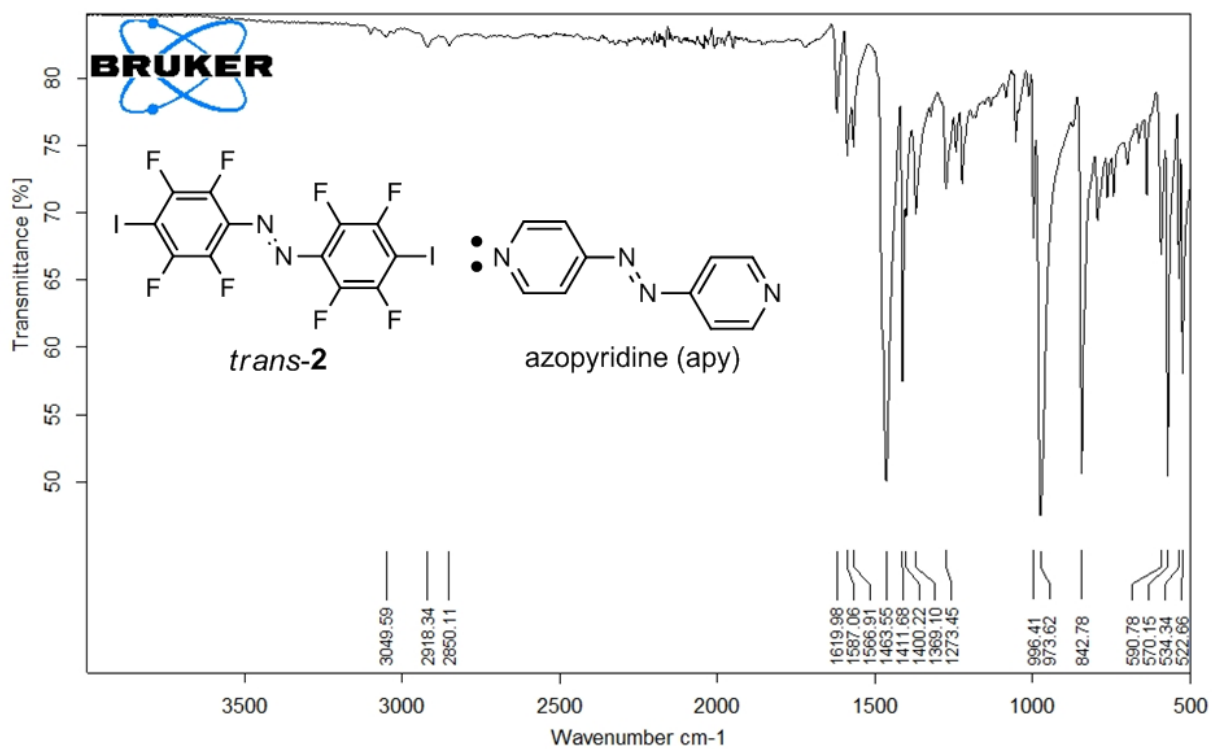


Figure S36. FTIR-ATR spectrum of (*trans-2*)(apy).

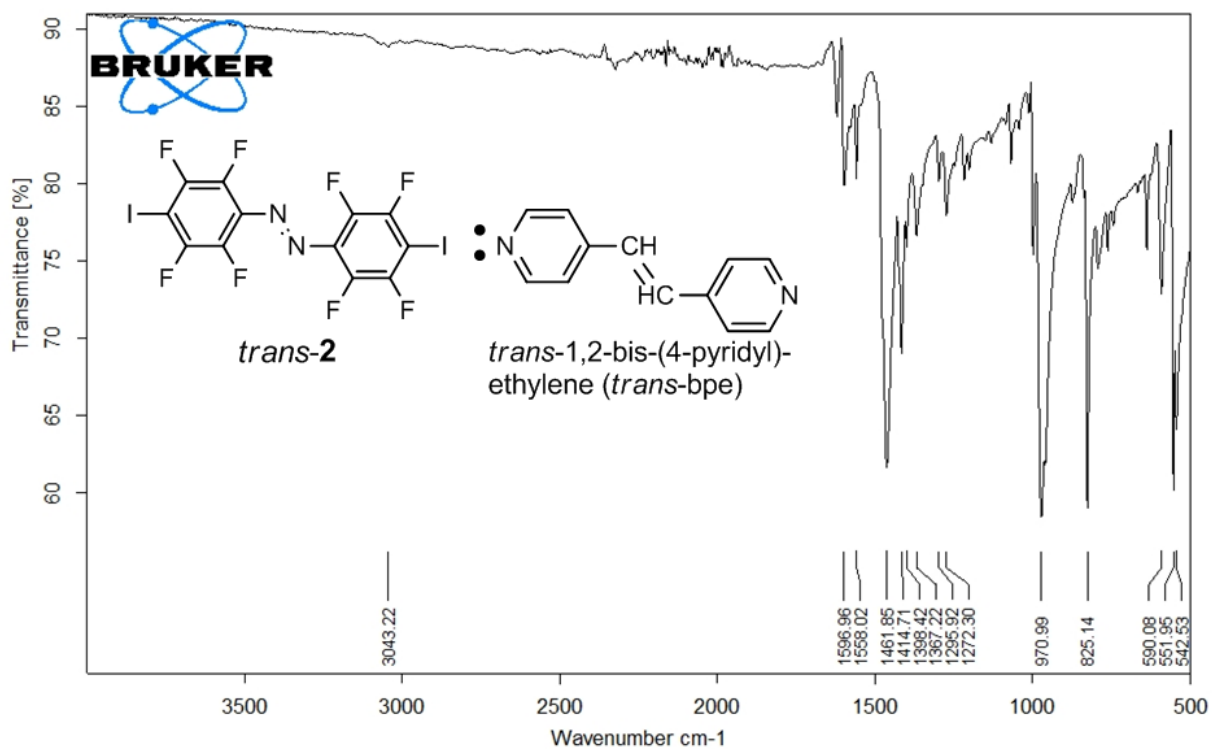


Figure S37. FTIR-ATR spectrum of (*trans-2*)(*trans-bpe*).

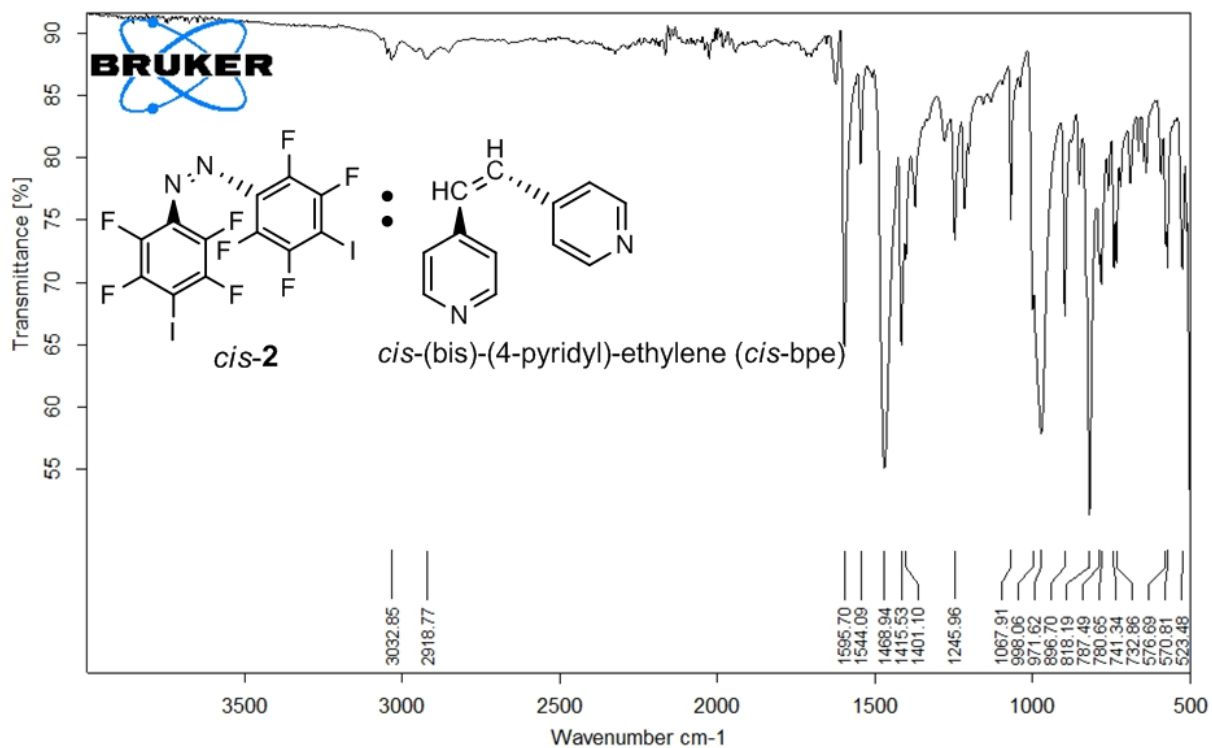


Figure S38. FTIR-ATR spectrum of  $(cis-2)(cis-bpe)$ .

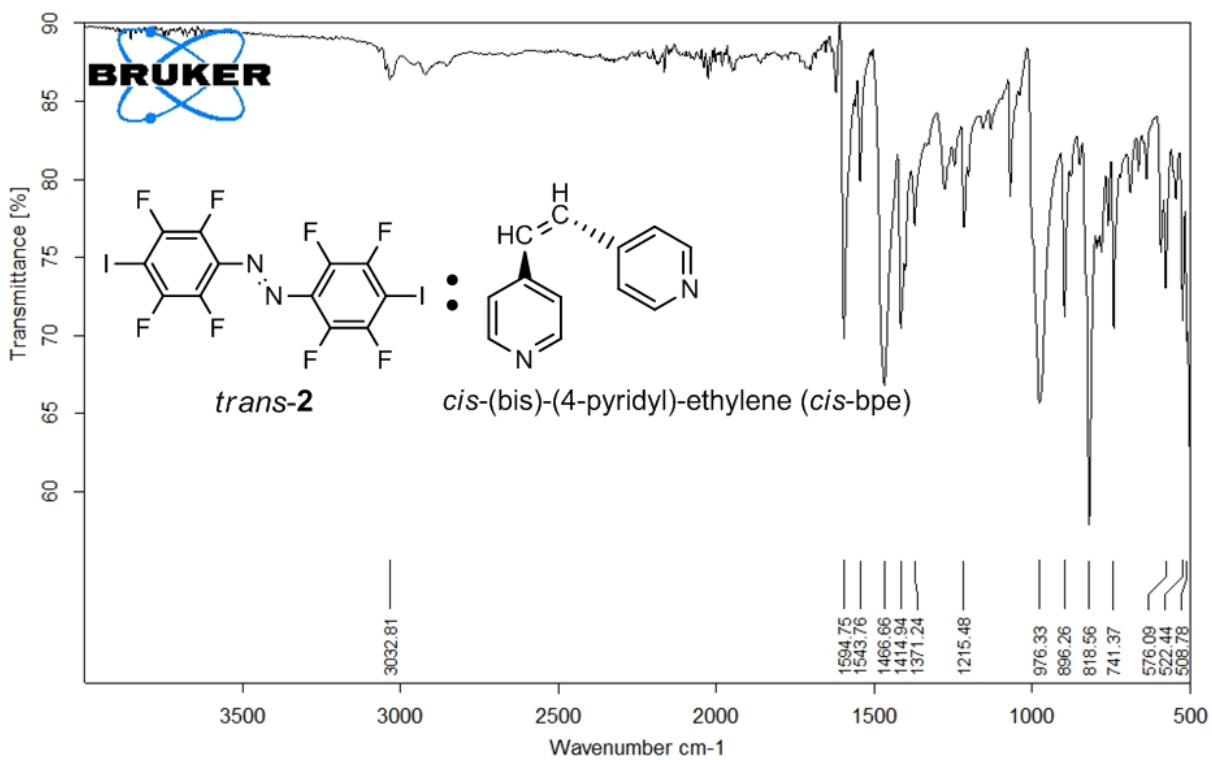


Figure S39. FTIR-ATR spectrum of  $(trans-2)(cis-bpe)$ .

## 8. References

- [1] Bushuyev, O. S., Tomberg, A., Friscic, T. & Barrett, C. J. Shaping Crystals with Light: Crystal-to-Crystal Isomerisation and Photomechanical Effect in Fluorinated Azobenzenes. *J. Am. Chem. Soc.* **135**, 12556-12559, (2013).
- [2] Sheldrick, G. M. *Acta Cryst.*, **2008**, *A64*, 112.
- [3] Sheldrick, G. M. (2004). *CELL\_NOW*. University of Göttingen, Germany.